

1 **Modelling storm-induced beach/dune**
2 **evolution: Sefton coast, Liverpool Bay,**
3 **UK**

4
5
6 Pushpa Dissanayake (Corresponding author)

7 *Energy and Environment Research Group, College of Engineering, Swansea University,*

8 *Singleton Park, Swansea, SA2 8PP, UK*

9 ++44(0) 1792 295540

10 ++44(0) 1792 295676

11 p.k.dissanayake@swansea.ac.uk

12

13

14 Jennifer Brown

15 *National Oceanographic Centre, Joseph Proudman Building, 6 Brownlow Street,*

16 *Liverpool, L3 5DA, UK*

17 jebro@pol.ac.uk

18

19

20 Harshinie Karunarathna

21 *Energy and Environment Research, College of Engineering, Swansea University,*

22 *Singleton Park, Swansea, SA2 8PP, UK*

23 h.u.karunarathna@swansea.ac.uk

24

25

26

27

28

29

30

31

32

33

34

35

36

37 **Abstract**

38

39 Storm-induced dune evolution on a sandy coastal system is investigated using a nested
40 modelling approach applied to the Sefton coast, Liverpool Bay, UK. Real-time offshore
41 water levels and waves were used as model boundary forcings. A Delft3D coarse grid
42 setup is used to simulate time and space varying sea surface elevations on which offshore
43 waves are transformed (by applying the SWAN model) to establish the wave boundary
44 for the high resolution morphological model (XBeach). Statistical comparisons between
45 model predicted and measured post-storm profiles at a number of locations along the
46 coast suggest that XBeach successfully captures storm-induced beach change along the
47 Sefton coast. Predicted bed evolution of the beach/dune system shows alternate erosion
48 and sedimentation areas in the nearshore. Strong bed level changes are found at the
49 northern part of the Sefton coast when north-westerly (NW) extreme waves and winds
50 coincide with spring-high tide. Morphological changes in the southern part are
51 significantly lower than that in the north as a result of NW wave dissipation on the shoals
52 located to the north of the Crosby channel, which creates low wave actions in that area.
53 In addition, erosion of the dune foot is observed at some locations along the beach.
54 Temporal simulation of beach/dune evolution as a result of variable forcing conditions
55 during storms provides useful insight into the morphodynamic processes of beach/dune
56 systems during storms (using Sefton as an example), which is very useful for developing
57 coastal management strategies over the existing conceptual tools.

58

59

60 Key words: *real-time boundary forcing, dune erosion, profile evolution, XBeach, Sefton*
61 *coast, Liverpool Bay*

62

63

64

65

66

67

68

69

70

71

72

73

74

75

76

77

78

79

80

81

82 **1. Introduction**

83

84

85 Coastal dune systems provide natural defence against erosion and flooding. They also
86 provide an important natural habitat to local flora and fauna (Carter, 1988). Development
87 and existence of coastal dunes are mainly controlled by cross-shore sediment transport
88 delivering sediment to the upper beach and then Aeolian transport reshaping deposited
89 sand (Harley and Ciavola, 2013). It is generally found that winter storms cause steep
90 cross-shore profiles by dune erosion and offshore sediment transport while calm, mild
91 summer conditions system recovery results in a more gentle profile shape in most of the
92 world's coastal systems (Callaghan et al., 2008). Severe storms in winter are responsible
93 for non-recoverable erosion leading to dune breaching and then subsequent flooding of
94 the hinterland areas.

95

96 There are four regimes of dune change during storm events depending on the water level
97 and the upper limit (the 2% exceedance level, R2%) of wave run-up heights (Sallenger,
98 2000). They are: 1) the swash regime – the dune system remains untouched, 2) the
99 collision regime – wave bores collide with the dune face, 3) the overwash regime – a
100 fraction of the waves overtop the dune crest and 4) the inundation regime – the dune is
101 completely submerged. Episodic slumping of the dune face occurs during the collision
102 regime (Palmsten and Holman, 2012; Erikson et al., 2007; Vellinga, 1986). The dune
103 crest height can be rapidly reduced during the overwash and inundation regimes because

104 sediment is transported both landwards and seawards from the dune (Donnelly et al.,
105 2006).
106
107 Storm-induced dune erosion is one of the major concerns of coastal safety and
108 sustainable development in the areas where frontal dune systems are present. In recent
109 years, there is growing attention to investigate and understand the storm driven dune
110 erosion processes in terms of numerical modelling approaches and statistical simulations
111 (Pender and Karunarathna, 2013; Callaghan et al., 2008; McCall et al., 2010; Lindemer et
112 al., 2010; Ranasinghe et al., 2011; Williams et al., 2011; Harley and Ciavola, 2013) due
113 to possible changes in future storminess.
114
115 Numerical modelling approaches have been developed over the last years in order to
116 predict more accurate and reliable dune evolution (Stive and Wind, 1986; Larson and
117 Kraus, 1989; Roelvink and Stive, 1989; Bosboom et al., 2000; Larson et al., 2004;
118 Roelvink et al., 2009). XBeach is one of the latest developments and an *off-the-shelf*
119 model which is being continually improved by applications in different coastal
120 environments around the world. This model has proven to be capable of predicting
121 morphodynamic storm impacts of beach/dune systems in numerous case studies
122 (Roelvink et al., 2009; McCall et al., 2010; Harley and Ciavola, 2013; Harley et al., 2011;
123 Lindemer et al., 2010; Splinter and Palmsten, 2012; Williams et al., 2011). These studies
124 motivated us to use and test the XBeach model to investigate storm driven beach/dune
125 evolution in hyper-tidal conditions along the Sefton coast, Liverpool Bay, UK.
126

127 In previous research, different methods have been carried out in Liverpool Bay and
128 specifically on the Sefton coast to hindcast and forecast wave climate, tidal-surge
129 propagation and morphological evolution (Jones and Davies, 1998; Esteves et al., 2012;
130 Brown et al., 2010a,b,c; Woodworth et al, 2007; Esteves et al., 2011; Wolf et al., 2011;
131 Wolf and Woolf, 2006; Pye and Neal, 1994; Pye and Blott, 2008; Brown et al., 2012;
132 Brown, 2010 and many others). Numerical models were mainly used to investigate the
133 hydrodynamic characteristics (wave climate, tide, surges and their interactions leading to
134 extreme events) under existing and future scenarios of sea level rise and climate change
135 locally and also over the larger scale of the Irish Sea (Brown et al., 2012; Brown et al.,
136 2010a,b,c; Wolf et al., 2011; Woodworth et al., 2007; Brown, 2010; Wolf and Woolf,
137 2006; Jones and Davies, 1998), to identify the importance of externally and locally
138 generated conditions to Liverpool Bay. Although these results are not directly applicable
139 to the Sefton coast, they provide potential offshore boundary conditions which can be
140 used to model the local morphodynamics. Only a few studies discuss morphological
141 evolution along the Sefton coast itself (Esteves et al., 2012; Williams et al., 2011; Esteves
142 et al., 2011; Esteves et al., 2009; Halcrow, 2009; Pye and Neal, 1994; Pye and Blott,
143 2008) and they have mainly focused on historical data analysis implying the general
144 patterns of morphological changes. Pye and Neal (1994) analysed the historical shoreline
145 changes from 1845 to 1990 and found that middle reaches of the Sefton coast is eroding
146 (~ 3 m/year) while northern and southern parts are accreting (~ 1 m/year). Decadal
147 variation in dune erosion and accretion from 1958 to 2008 was investigated by Pye and
148 Blott (2008) using a series of beach and dune surveys. This analysis shows that severe
149 dune erosion occurs when storms generate positive surges on several successive tides.

150 Esteves et al (2012) have quantified water level, significant wave height and dune erosion
151 on the Sefton coast during several historical storm events and developed linear
152 relationships among them in order to establish a threshold condition for dune erosion. In
153 their study, dune erosion was estimated using one-dimensional (1D) profile data and they
154 emphasized that inclusion of alongshore variation in the beach/dune morphology (i.e. 2D
155 approach) is important to investigate dune evolution during stormy conditions. The
156 MICORE project (Ciavola and Jimenez, 2011; Williams et al., 2011) has specifically
157 focused on the storm driven dune erosion and potential hinterland flooding on the Sefton
158 coast. They adopted the XBeach model (in 1D and 2D) imposing time-invariant wave
159 boundary conditions (i.e. single wave condition) over a tidal cycle in a localised model
160 domain for each tested scenario. These boundary forcings imply a conservative approach
161 compared with the real-time storm-driven forcings and thus could lead to overestimation
162 of morphodynamic changes of the beach/dune system.

163

164 The objective of the present study is to investigate the spatial variability of the exchange
165 of sediment between dune face and beach during a storm, and to examine the alongshore
166 variability of sediment dynamics in determining the evolution of the Sefton beach/dune
167 system at engineering timescales. Such information is vital in taking effective and
168 sustainable coastal management decisions.

169

170 There are a number of coastal management practices on the Sefton beach/dune system
171 implemented by the Sefton Metropolitan Borough Council to deal with nature
172 conservation and land management, shoreline management, coastal defence and flood

173 risk, recreation, leisure and tourism (Houston, 2010; McAleavy; 2010). Success of these
174 strategies depends on the understanding of how this complex beach/dune system interacts
175 with coastal processes not only over the long-term, but also during storm conditions, with
176 focus on the spatial and temporal variation of the resulting sediment fluxes and in turn the
177 morphological changes. Application of numerical models is very efficient and effective in
178 order to get such high resolution details of the beach/dune system. Previously, an event
179 scale 1D early warning system for erosion has been developed for Formby Point (Souza
180 et al., 2013). In this paper a 2D application of numerical models is used to identify the
181 processes causing storm driven morphological change to support conceptual modelling
182 based on beach monitoring that informs the local shoreline management plans. This
183 research will therefore supplement the bi-annual beach surveys carried out by the Sefton
184 Metropolitan Borough Council by providing detailed information of storm impacts at the
185 individual event scale, in addition to the seasonal observations that capture the longer
186 term beach and dune response.

187

188 In this study a nested modelling approach is used. A larger, coarse grid, 2D model
189 domain is used to transform real-time offshore boundary forcings into the nearshore area.
190 A high resolution, smaller domain, which represents the initial bed topography and in
191 turn the resulting erosion and sedimentation patterns, is set up to investigate storm-
192 induced dune evolution along the Sefton coast. Implementing real-time boundary forcing
193 in the model allows more realistic storm induced interactions between the hydrodynamics
194 and morphodynamic evolution.

195

196 This paper is structured as follows. Section 2 and 3 describe the study area and the
197 selected storm event respectively. Section 4 describes the modelling approach used to
198 obtain the results given in section 5. A discussion of the overall findings is present in
199 section 6 while section 7 provides conclusions.

200

201

202

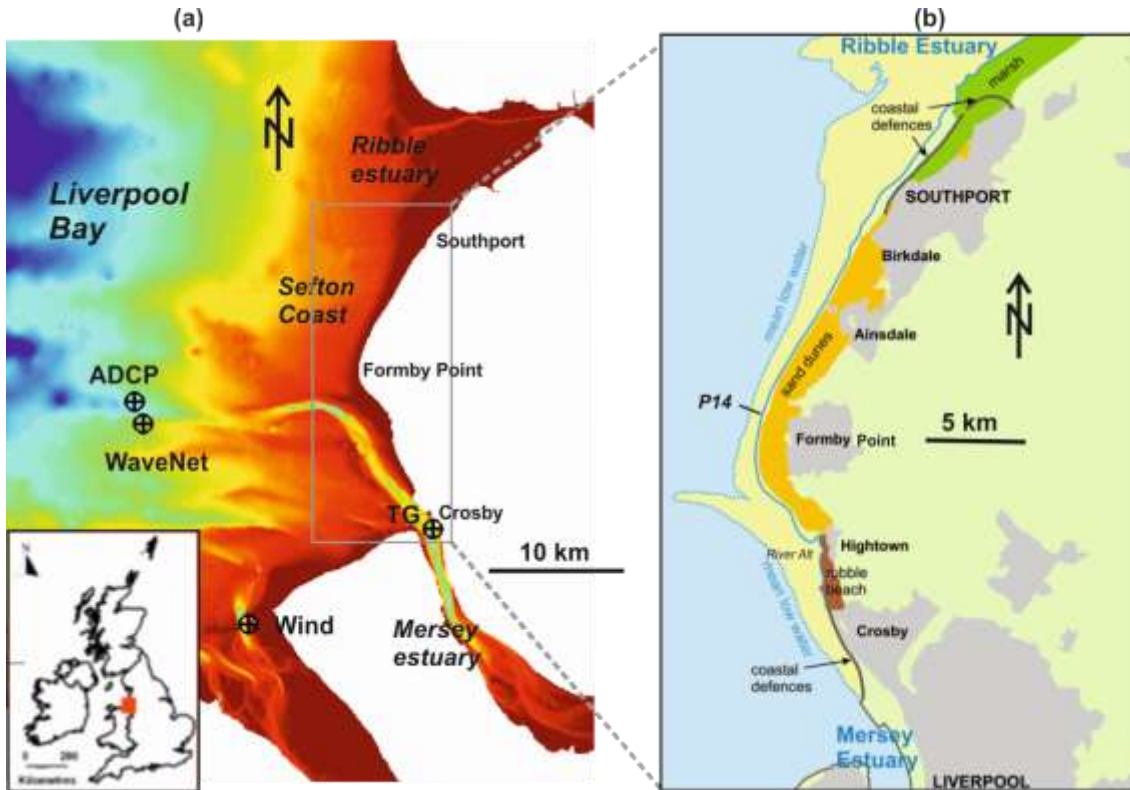
203

204 **2. Study area - Sefton coast**

205

206 The Sefton coast is located between the Mersey estuary (to the south) and the Ribble
207 estuary (to the north) in Liverpool Bay. It is an approximately 36 km long convex shape
208 coastal stretch (Figure 1a) (Williams et al., 2011; Brown et al., 2010a,b; Pye and Blott,
209 2008; Plater and Grenville, 2010). The Sefton coastal system consists of natural
210 beaches/dunes which have high recreational and nature conservational value, engineered
211 beaches protected by seawalls, groynes and revetments and, rubble beaches covered with
212 building material debris and rock armours (Figure 1b). The dunes within the system
213 extend about 4 km inland, reach about 30 m ODN in height at some locations and
214 represents around 20% of the entire UK dune population (Souza et al., 2013; Esteves et
215 al., 2012; Williams et al., 2011; Pye and Blott, 2010; Esteves et al., 2009). These dunes
216 form an effective natural coastal flood defence for the local urban areas, high grade
217 agricultural lands and a significant number of conservational areas of national and
218 international interest. It also consists of extremely high biodiversity that includes rare and

219 endangered species (Edmondson, 2010; White, 2010; Smith, 2010). Growth and
 220 existence of these highly valued natural systems depends on the sustainability of the
 221 beach/dune system, which is currently under threat due to erosion and nearby manmade
 222 developments.
 223



224
 225 **Figure 1 (a) Location of Liverpool Bay and Sefton coast with data observation points; ADCP**
 226 **(offshore tide), WaveNet (offshore wave characteristics), TG (Liverpool Gladstone Dock, nearshore**
 227 **tide) and Wind (Hilbre wind station) (b) a close-up of the Sefton beach system and the P14 profile**
 228 **location.**

229
 230 The tidal regime at Liverpool Bay consists of an alongshore propagating semi-diurnal
 231 hyper-tide with a mean spring tidal range reaching about 8.2 m at Liverpool Gladstone
 232 Dock (see location *TG* in Figure 1a) (Brown et al., 2010a; Palmer, 2010; Blott et al.,

233 2006). Using long term wave measurements at an offshore location in Liverpool Bay (see
234 location *WaveNet* in Figure 1a), Brown et al (2010b) simulated an 11-year wave hindcast
235 which suggests a mean annual significant wave height (H_{m0}) of 0.5 m, with extremes
236 reaching 5.6 m. The mean annual peak wave period (T_p) is 5 s while extremes are about
237 22 s. Positive surge in the area is often less than 0.5 m, however, during stormy
238 conditions extreme surges of 2.4 m have been recorded along the Sefton coast (Brown et
239 al., 2010a). The largest surges generally occur during lower water levels (i.e. rising tide).
240 The maximum surge recorded at high water (i.e. 5.6 m) in Liverpool Bay is about 2 m in
241 1976 (Brown et al., 2010a). The largest wave conditions are associated with west to
242 north-west winds where the longest fetch exists (Wolf et al., 2011).

243

244 Sediment characteristics of the Sefton coast are determined by inflow of the Mersey and
245 Ribble estuaries, in addition to the net onshore drift due to the tides (Pye and Blott,
246 2008). Sediment composition in the nearshore area varies from about 0.1 mm to 0.3 mm
247 in median grain size (D_{50}) (per. comm. with Sefton Metropolitan Borough Council).
248 However, sediment information in the beach/dune system is very scarce. An average
249 sediment size of 0.2 mm is used for the entire domain in the present model runs. The
250 inter-tidal area of the Sefton coast has a ridge runnel system, which extends about 3 km
251 seaward over a beach profile with a very mild slope of about 1:100 (Plater and Grenville,
252 2010).

253

254 The primary mechanisms leading to dune erosion are the soaking of the dune toe and then
255 wave undercutting which can lead to slumping of the dune face and dune retreat (Pye and

256 Blott, 2008; Parker, 1969). The Sefton dune foot is located just above the mean spring
257 high water level. Therefore, dune erosion occurs when extreme storm surge and wave
258 events coincide with the spring-high tide. However, there is a potential for significant
259 erosion during storm surges with high wave energy (Halcrow, 2009; Pye and Blott,
260 2008). Smaller storms erode only part of the Sefton coast while erosion of the entire dune
261 frontage is possible during the most severe (> 1 in 10 year) events (Pye and Blott, 2008).

262

263 Metocean conditions in Liverpool Bay together with the shape of the coastline (i.e.
264 convex shape) and the beach slope result in different morphological evolution along the
265 Sefton coast. Some parts experience erosion while others accrete with different rates and
266 trends (Esteves et al., 2012; Pye and Blott, 2008; Pye and Neal, 1994). The area around
267 Formby Point (see Figure 1b) is highly dynamic. Prior to 1900, this area suffered seaward
268 progradation, however it turned into an eroding system around the beginning of the 20th
269 century (Pye and Neal, 1994; Pye and Smith, 1988; Gresswell, 1953). Local beach/dune
270 erosion at Formby Point delivers sediment to the accreting shorelines both northward and
271 southward (Halcrow, 2009; Pye and Blott, 2008; Pye and Neal, 1994). As a result,
272 Formby Point presently acts as a divergent sediment cell boundary. Esteves et al (2009)
273 found that the annual dune retreat north of Formby Point is about 5 m during the period
274 from 2001 to 2008 and the erosion extends up to the River Alt area (see Figure 1b).

275

276

277 **3. Storm event**

278

279 A storm event that occurred between 29 March 2009 and 01 April is modelled in this
280 study. The selection of this event was purely based on the availability of pre-storm
281 (Sefton Metropolitan Borough Council) and post-storm (Williams et al., 2011) beach
282 profile measurements for model calibration. It should be noted that even though a
283 significant number of profile measurements are available for the Sefton coast, the timing
284 and frequency of surveys prevents accurate pre and post storm observations, limiting
285 their use for the current modelling purpose. In order to find out the severity of this storm
286 event a comparison of its estimated storm power (Dolan and Davies, 1994; Karunarathna
287 et al., 2014) with all historical events between 2003 and 2011 was made. This analysis
288 categorised the presented event as ‘*medium*’ severity.

289

290 The measured meteorological conditions (tide, wave and wind) in Liverpool Bay are
291 shown in Figure 2 for the period from 27th March to 05th April 2010. Tidal elevations are
292 shown for two locations, an offshore point at 24 m ODN depth (i.e. see location ADCP in
293 Figure 1a) and a tide gauge station inside the Mersey estuary (i.e. Liverpool Gladstone
294 Dock tide gauge, see location TG in Figure 1a). The tide gauge data represents nearshore
295 water levels for the Sefton coast while the ADCP provides offshore water level
296 variations, which are later used as model boundary forcing (see section 5.1). Both water
297 level time series are referenced to mean sea level (MSL) (see Figure 2a). Observations
298 indicate that Liverpool Bay experiences spring-tides during this period. Differences in
299 amplitudes and phases of these two tidal signals are expected due to the effects of local
300 bathymetry in the shallow area and the geometry of the Mersey estuary (Dronkers, 2005).

301

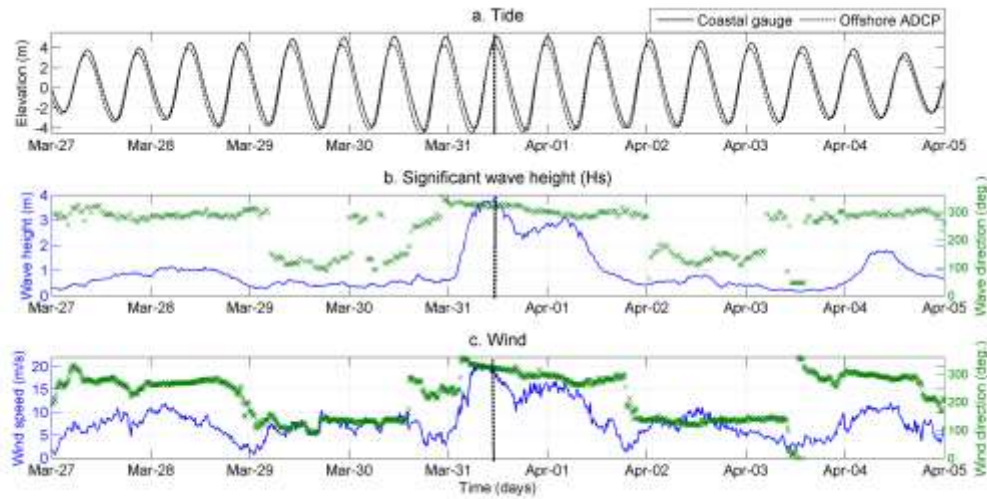
302 Wave characteristics during this period are determined from the Liverpool Bay WaveNet
303 buoy (i.e. Directional Waverider MkIII, serial number 30897) located at 24 m ODN depth
304 (see location WaveNet in Figure 1). Significant wave height (H_s) shows a double-peak of
305 which the maximum occurs on the 31st March (Figure 2b). The maximum recorded H_s of
306 this storm is 3.80 m as it approaches from a north-westerly (NW) direction (i.e. 318° , see
307 Figure 1b). Occurrence of this wave height is marked with a dash-line for all parameters
308 in Figure 2. According to the tidal elevations, the maximum wave height coincides with
309 High Water (HW) (i.e. 4.76 m ODN at Gladstone Dock). The position of the dune toe
310 generally lies slightly above the mean high water spring level (MHWS ~ 4.39 m ODN)
311 and slightly increases towards the Ribble Estuary (Pye and Blott, 2008). Therefore, it can
312 be expected that the dune toe may be subjected to soaking depending on the local
313 morphology and the total water level while exposed to wave attack. At lower tidal phases
314 strong local winds (i.e. wind speed is about 20 m/s, see Figure 2c and gusts exceeding 25
315 m/s, not shown), blowing from a NW direction (320°), develop more aggressive wave
316 action on the beach/dune front. Such a combination of forcing conditions (i.e. tide, wave
317 and wind) is expected to result in significant morphological changes along the Sefton
318 coast. It is noted that the occurrence of high waves coincidental with HW and a strong
319 winds is not typically found in the historical in Liverpool Bay storm records (Esteves et
320 al., 2012). Therefore, the present storm event is considered appropriate to undertake a
321 morphological investigation.

322

323

324

325



326

327 **Figure 2** Variation of meteorological conditions from 27 March to 05 April 2010; Tide (a), Significant
 328 wave height (b) and wind (c). The vertical dashed-line represents the peak of the storm event.

329

330

331

332

333 **4. Model setup**

334

335 A nested modelling approach is setup in order to optimize the computational time and
 336 accurately represent the nearshore topography (i.e. beach/dune system). Our study
 337 primarily applies the XBeach model (Roelvink et al., 2009) to investigate the storm
 338 impact on the beach/dune evolution while the SWAN (Booij et al, 1999) and Delft3D
 339 (Lesser et al., 2004) models are implemented to establish boundary forcings. The Delft3D
 340 model is used to develop spatial and temporal varying sea surface elevations and velocity
 341 fields. These parameters are subsequently applied into the SWAN model in order to

342 transform offshore waves up to the XBeach model boundary imposing wave-current
343 interactions under real-time water levels.

344

345

346 **4.1 Model domains**

347

348 *One – dimensional (1D) model domain*

349

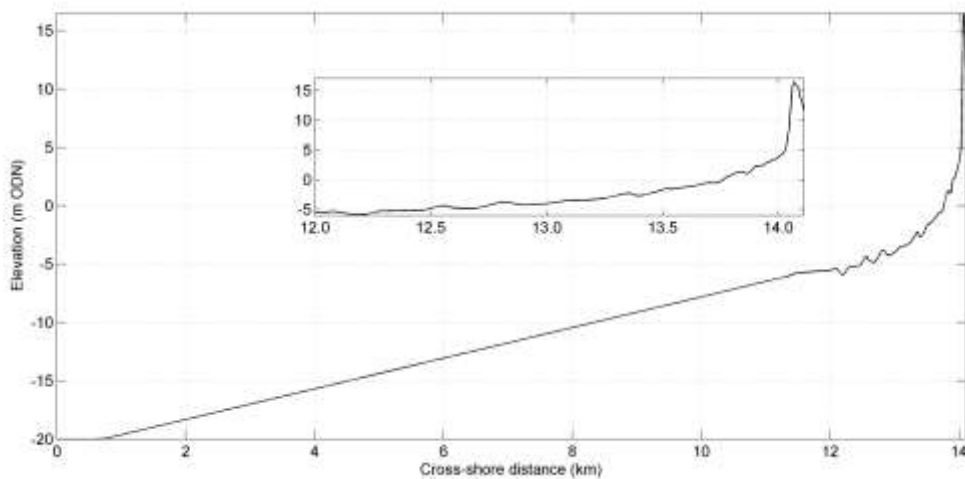
350 The sensitivity tests described in section 4.4 use a 1D approach to simplify the situation
351 and to minimise excessive computation times to evaluate the large number of model
352 parameters involved. Even though this approach has some consequences, the cross-shore
353 profile used for the sensitivity analysis is considered as a representative profile of the
354 Sefton beach (see Figure 1b, *PI4* is located at Formby Point) due to two main reasons.
355 Firstly, it is located at a point of diverging alongshore sediment transport, so is
356 representative of the cross-shore sediment dynamics, and is in a highly dynamic area of
357 the Sefton coast, which undergoes strong morphological change compared with other
358 locations along the coast (Esteves et al., 2012; Pye and Blott, 2008). Secondly, only this
359 profile has measurements that extend up to about -8 m ODN depth. All other profiles
360 have the seaward measurement limit up to about -2 m ODN only.

361

362 A pre-storm cross-shore profile at *PI4* measured on the 14th March 2010 was established
363 using available historical profile data from 1996 to 2010 and LiDAR data (Gold, 2010).

364 The profile data are measured by the Sefton Metropolitan Borough Council, with the

365 addition of the event-scale monitoring undertaken by the MICORE project (Williams et
366 al., 2011) for this case. These latter profile measurements have a cross-shore resolution of
367 minimum of 5 m in the beach/dune area. The nearshore beach/dune profile (from dunes
368 to -2 m ODN depth) was defined by the pre-storm LiDAR data which has a resolution of
369 1 m \times 1 m in horizontal and about ± 15 cm uncertainty in vertical. The profile from -2 m
370 to -8 m ODN depth was determined from this historical data. The profile was then
371 extended to -20 m ODN using a straight line (Figure 3). The profile consists of nearshore
372 bar-trough patterns up to about -6 m ODN and a constant slope of about 1:500 thereafter.
373 The computation domain was extended up to an offshore depth of -20 m ODN in order to
374 generate offshore boundary conditions accurately (per. comm. with Deltares XBeach
375 team). The offshore grid resolution was selected as 10 m, while a higher grid resolution
376 (~ 2 m) is used over the beach/dune area.
377



378
379 **Figure 3 Established pre-storm 1D profile at location P14 (see Figure 1) for the sensitivity analysis**
380

381

382

383 *Two – dimensional (2D) model domain*

384

385 A 2D model domain is used for morphodynamic simulations of storm-induced beach
386 dune evolution. A nested modelling approach adopted in this study uses the *Sefton* and
387 *Formby* model domains as shown in Figure 4. The *Sefton* model domain is used to
388 transform offshore hydrodynamics (tides and waves) up to nearshore. Morphological
389 changes around the Formby Point area are investigated using the *Formby* model domain.
390 Both domains consist of curvilinear grids which follow the convex shape of the Sefton
391 coastline and the dune topography. Grid resolution in both models was varied across the
392 domain in order to achieve higher resolution in the areas of interest. The spread of the
393 offshore boundary is designed to capture all incident wave directions influencing this
394 coastal stretch.

395

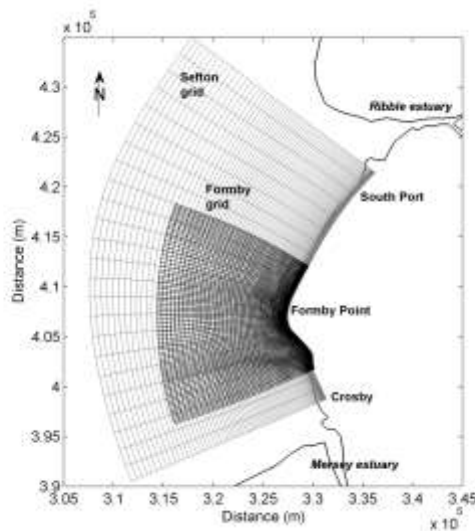
396 The *Sefton* domain is established in both Delft3D and SWAN in order to provide water
397 level, velocity and wave boundary conditions for the smaller *Formby* domain. The latter
398 extends from Crosby (in the south) to Southport (in the north) covering a stretch of about
399 26 km representing almost the entire Sefton coast (Sefton grid in Figure 4). The location
400 of the offshore boundary is based on the Liverpool Bay *WaveNet* buoy (see Figure 1) of
401 which measured wave data are imposed in the SWAN model. Accordingly, the lateral
402 extension of this model is about 23 km offshore and the length of the offshore boundary
403 is about 45 km. Fairly coarse grids are applied in both x and y directions (minimum grid
404 $25\text{ m} \times 650\text{ m}$ and maximum grid $300\text{ m} \times 800\text{ m}$) compared with the *Formby* model as

405 this is only applied to transform offshore hydrodynamic characteristics (i.e. waves and
406 tides) for the XBeach simulations.

407

408 The *Formby* model domain covers the highly dynamic beach/dune system around
409 Formby Point which extends about 12 km in the alongshore direction. The depth of the
410 offshore model boundary was defined by applying the depth of closure approach of
411 Hallermeier (1983), assuming that no morphological changes occur beyond this point (i.e.
412 $d_{doc,outer} < 15$ m). This results in lateral extension of the model domain 15 km offshore.
413 High resolution grid cells (~ 2 m \times 25 m in cross-shore \times alongshore directions) are
414 applied in the beach/dune area in order to resolve the dune shape adequately into the
415 model while coarser grid cells (~ 150 m \times 110 m) are used offshore. Such grid
416 arrangements optimize the computational time which is an advantage for morphological
417 simulations.

418



419

420 **Figure 4 Model domains applied in this study with the land boundary; XBeach finer grid setup**

421 **(Formby grid, dark grey) and Delft3D/SWAN coarser grid setup (Sefton grid, light grey)**

422

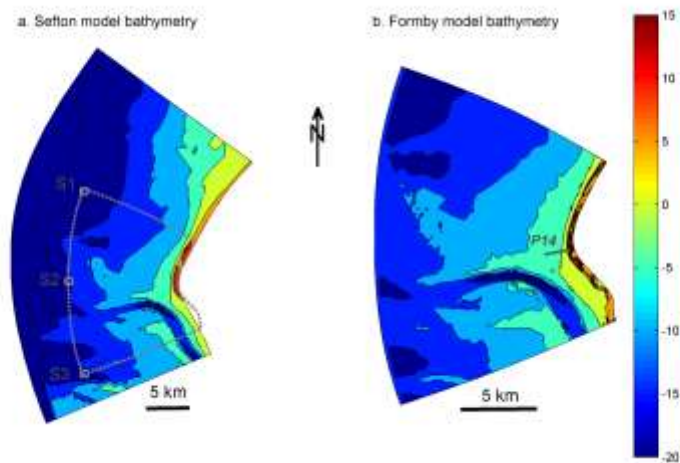
423 **4.2 Sea bed bathymetry**

424

425 Sea bed bathymetry and the dune topography for the 2D model were determined from the
426 existing hydrodynamic model POLCOMS (Brown et al., 2010a) and the LiDAR data set
427 (Gold, 2010) respectively. The 90 m resolution POLCOMS bathymetry has been
428 established using previous bathymetric data available in Liverpool Bay (i.e. from 2000 to
429 2008) and extends from the Sefton dune system (5 m ODN) to an offshore depth of about
430 -50 m ODN (Williams et al., 2011). The LiDAR data set is based on the airborne laser
431 scan transects observed on the 14th March 2010 (Gold, 2010). It has 1 m × 1 m resolution
432 and covers the entire dune system up to about -2 m ODN depth. LiDAR data were re-
433 gridded to 2 m × 2 m resolution to be used in our model. High resolution LiDAR data
434 provides the model bathymetry from dune crest to -2 m ODN. The rest of the bathymetry
435 (depth < -2 m ODN) was determined from the POLCOMS model bathymetry. The
436 offshore boundary of the *Sefton* model is located at -25 m ODN (i.e. location of the
437 *WaveNet* buoy, see Figure 1) while that of *Formby* was set at -15 m ODN (i.e. $d_{doc,outer} <$
438 15 m) (Figure 5). It is noted that the offshore uniformity for boundary forcings is
439 maintained in both cases by using a constant depth along the boundaries.

440

441



442

443 **Figure 5** Model bathymetries developed based on LiDAR data and POLCOMS model bed for the
 444 *Sefton* domain (a) with outline of the *Formby* model and observation locations (S1, S2 and S3) , and
 445 *Formby* domain (b) with the location of profile P14

446

447

448

449 **4.3 Boundary forcings**

450

451 Boundary forcings for the model simulations were formulated in order to generate the
 452 hydrodynamic characteristics of the selected storm event (see Figure 2). The
 453 implemented real-time forcing conditions in this study are 1) *Tide*, 2) *Surge*, 3) *Wave* and
 454 4) *Wind*.

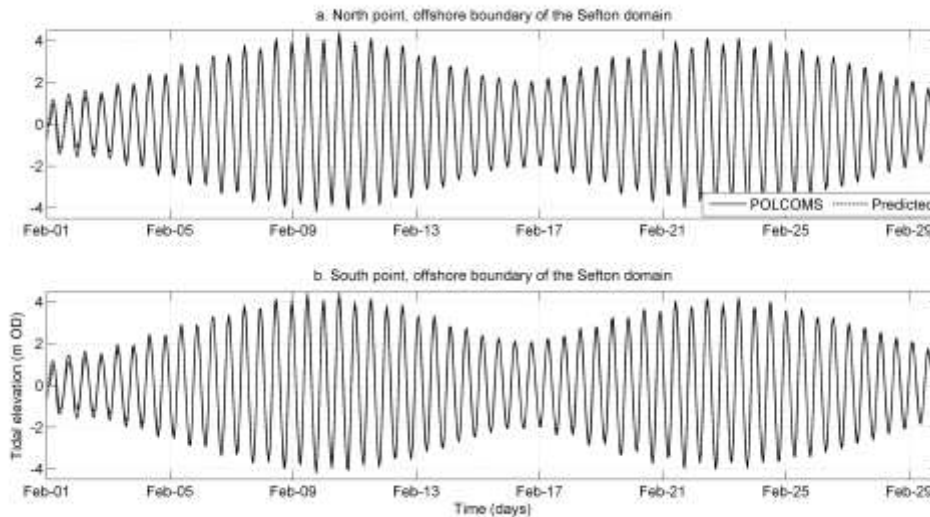
455

456

457 *Tide*

458

459 The total water elevation boundary conditions for the *Formby* model were extracted from
460 those simulated by the *Sefton* model. The tidal boundary conditions for the *Sefton* model
461 were obtained from the ADCP data (see location *ADCP* in Figure 1a). It should be noted
462 that the alongshore propagating tide at Liverpool Bay has alongshore tidal phase
463 difference between the lateral (north and south) model boundaries. As there are no
464 observed data at the two lateral boundaries, the phase difference was estimated using
465 available POLCOMS model results in February 2008 (Bricheno et al., *in press*). Initially,
466 tidal elevations at the north and south points of the *Sefton* model were extracted from
467 POLCOMS . Each tidal signal was decomposed into tidal constituents applying a Fast
468 Fourier Transformation (FFT, i.e. observed sea surface is denoted by a number of tidal
469 constituents (~ 35) in their amplitude and phase differences) and then the corresponding
470 signals were reproduced for the same period using these estimated constituents (i.e.
471 Astronomical tide). Extracted tidal elevations from the POLCOMS results at north and
472 south points are shown in Figure 6 in comparison to the corresponding predicted
473 Astronomical tides which indicate sufficient agreement with the POLCOMS tide though
474 they imply marginally lower tidal range initially.
475



476

477 **Figure 6 Comparison of tidal elevations in February 2008 from POLCOMS results and Predicted**
 478 **tide at north (a) and south (b) offshore points of the *Sefton* model**

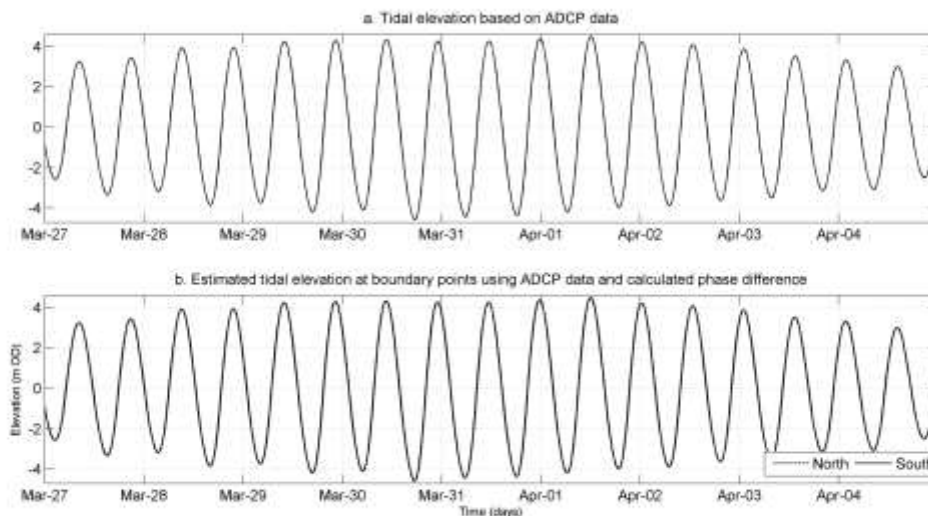
479

480 These estimated tidal constituents (~35) are subsequently adopted to predict the tidal
 481 elevations at those offshore points (i.e. north and south) during our study period (i.e. 27
 482 March to 05 April 2010). These two signals indicated, tidal elevation at the north point
 483 has a forward phase shift of 08 minutes and 38 seconds compared with that of the south
 484 point, confirming an alongshore propagating tide (i.e. from south to north) at the coast in
 485 this study area (Brown et al., 2010a). The ADCP provides observed total water depth at
 486 the offshore boundary (i.e. 24 m ODN depth at ADCP, see Figure 1a) during the selected
 487 storm event. For the storm event, these data were transformed into sea surface
 488 fluctuations with respect to MSL by removing the long-term (10-year) mean (see Figure
 489 7a). This approach allows the externally generated surge and tide to be included within
 490 the boundary elevations along with interaction. Total water elevations at the north and
 491 south offshore points of the *Sefton* domain were then determined applying the estimated
 492 tidal phase shift to the observed water elevation (see Figure 7b). The ADCP data

493 represents tide, surge and any interactions that have occurred along fetches to this point.
494 To capture any surge generation beyond this point the data is combined with tide gauge
495 observations.. To do this the difference (-0.2 m) between the long-term mean water
496 elevation and that during the storm event is used to bias the total time-varying water
497 elevation during the storm period to remove the mean increase in water level due to the
498 surge. By reconstructing a total time-varying surge component from tide gauge data, as
499 described below, not only allows the locally generated surge to be included but also
500 allows the total water elevation to be reference to ODN as required by the model. The
501 resulting water elevations so far therefore include the spatially varying tide and the tide-
502 external surge interactions relative to MWL.

503

504



505

506 **Figure 7 Measured ADCP data in the study period referring to MSL (a) and constructed tidal levels**
507 **for north and south offshore points of the *Sefton* model (b). Note, a phase-shift of 08 minutes and 38**
508 **seconds between North and South boundaries is hard to differentiate.**

509

510

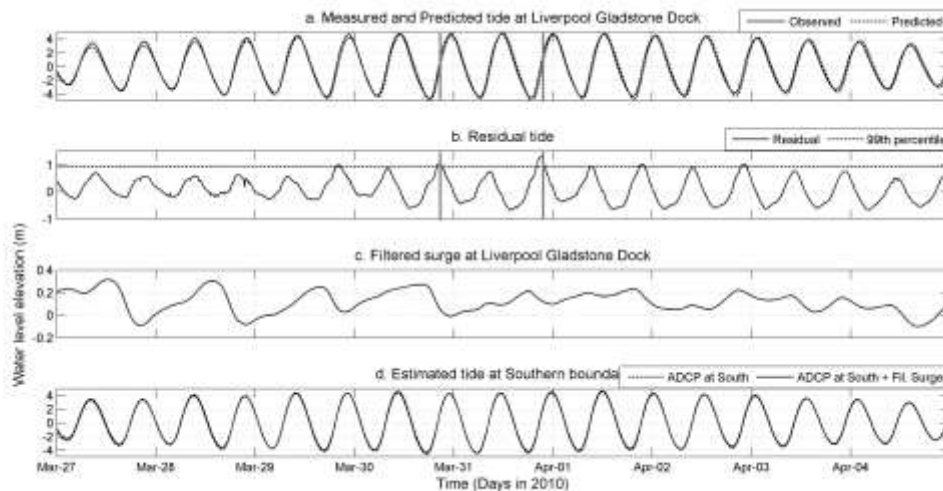
511 *Time-varying surge component*

512

513 The surge boundary forcing was estimated based on the observed tidal elevations at the
514 Liverpool Gladstone Dock tide gauge (TG in Figure 1a). The tidal elevation is referenced
515 to CD so can be analysed to create a surge elevation relative to ODN. Initially, the
516 observed tide was decomposed into 35 tidal constituents (i.e. applying FFT, see section
517 *Tide* above). Then, the Astronomical tide was predicted for the same period. The
518 observed elevation is the result of interactions between the propagating tidal wave,
519 meteorological forcings and bathymetry, while the extracted Astronomical tide represents
520 the sea surface variation without any local interference. It can be seen in Figure 8a that
521 the observed total elevation is marginally higher and travels faster (i.e. forward phase
522 shift) than the predicted tide. The difference between the two tidal signals is defined as
523 the residual elevation (Figure 8b) at the gauge location. In the present analysis, the
524 residual tide varies from -0.67 m to 1.29 m during the storm event and represents the total
525 time-varying surge influencing the coast (Figure 8b). The 99th percentile value of the
526 long-term residual elevation (horizontal dash line in Figure 8b) indicates the threshold for
527 extreme surge elevations which allow strong wave action on the dune front. The
528 estimated (0.93 m) 99th percentile value is exceeded twice (see grey vertical lines in
529 Figure 8a and b) during the storm period at times that coincidence with the rising tide. It
530 is typically found in Liverpool Bay that the maximum residual occurs during the rising
531 tide rather than at HW (i.e. when the observed tide travels faster than the predicted
532 Astronomical tide, see Horsburgh and Wilson, 2007). It is incorrect to superimpose this

533 residual elevation on to the offshore estimated total elevations (see Figure 7b) to
534 incorporate the surge into the model boundary forcings because any tide-surge interaction
535 occurring prior to the ADCP location would be double counted. To obtain the total time-
536 varying surge component without tide-surge interaction the observed water level at the
537 tide gauge was screened with a low-pass filter (see Dissanayake, 2011) to remove all
538 oscillatory components occurring within a tidal period (i.e. 745 minutes). The resulting
539 filtered surge varies between -0.09 m to 0.31 m in this storm event (Figure 8c) and
540 represent the time-varying MSL of the region and can therefore be combined with the
541 previously calculated water elevations (from the ADCP data) to represent the full tide-
542 surge conditions.

543
544
545



546
547 **Figure 8 Estimating tide and surge elevation for the model boundary; Measured and Predicted**
548 **(Astronomical) tide at Liverpool Gladstone Dock (a), Residual tide (b), Filtered tide at Liverpool**
549 **Gladstone Dock (c) and Estimated tide and surge at southern boundary of Formby domain (d)**

550

551

552

553 *Waves*

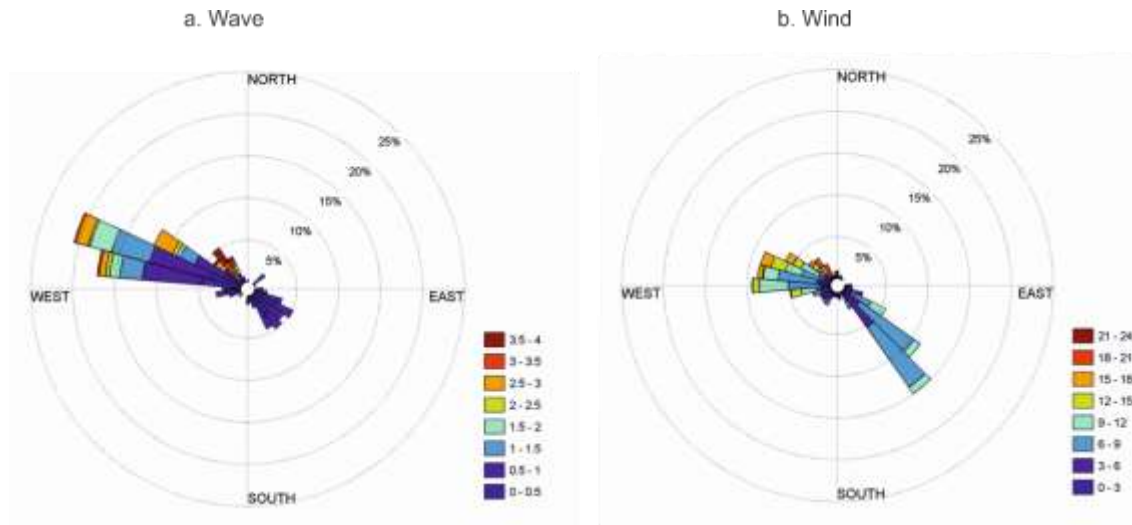
554

555 Offshore wave characteristics for the *Sefton* model boundary were derived using the
556 measured wave data from the WaveNet buoy. Wave data are available from 2002 to
557 present day (2013), covering an 11-year period. Analysis of this data set shows that the
558 highest probability of occurrence is in the 270° to 300° directional sector (~WNW). Wave
559 height rarely increases more than 5 m, typically exceeds 4 m during 1 – 5 events/year and
560 3 m during 5 – 10 events/year, while waves in the range of 0 – 1 m commonly occur each
561 year. Wave characteristics during the study period (27 March to 04 April 2010) are
562 shown in Figure 9a. The general trend of the long-term wave climate (i.e. from 2002 to
563 2013) is found even in this short period: High waves (> 1 m) occur in the North-West
564 quadrant. The dominant wave direction (i.e. highest probability of occurrence) is from
565 WNW whereas the highest waves (> 3.5 m) approach from a north-westerly direction.

566

567

568



569

570 **Figure 9** Wave and wind characteristics during the study period from 27 March to 04 April 2010;

571 **Wave rose (a) and Wind rose (b)**

572

573

574

575 *Wind*

576

577 Wind forcing is applied to the *Sefton* (i.e. wave/tidal transformation) and *Formby* (i.e.

578 morphological evolution) models based on observations from the Hilbre Island weather

579 station (see location *Wind* in Figure 1) to generate local waves. Any wind driven surge

580 generated within the model will be minimal due to small domains. The wind observation

581 sensors are mounted at approximately 10 m above the ground on a tower which is above

582 16.5 m ODN. The wind rose in Figure 9b shows wind speed and direction during the

583 study period. Strong winds (> 12 m/s) blow from the NW while wind speeds higher than

584 20 m/s approach from a NNW direction ($\sim 335^\circ$). In contrast to the wave data, the

585 dominant wind direction during the study period is from SE. This is due to the met station

586 being located at the mouth of the Dee estuary, which is aligned NW-SE, funnelling the
587 local wind. Wind data are applied at each grid cell of both model domains (*Sefton* and
588 *Formby*) such that they are spatially constant but temporally varying.

589

590

591

592 **4.4 Model Simulations**

593

594 Model simulations consist of three stages; 1) *Generating boundary forcings*, 2) *Sensitivity*
595 *analysis* and 3) *2D area modelling*. The simulation length spans from 27 March to 04
596 April 2010. It is noted that the measured beach/dune topography at 14 March 2010 (i.e.
597 re-gridded LiDAR data of 2 m × 2 m resolution) was considered as the initial pre-storm
598 beach-dune topography. This is justified by the fact that incident wave conditions during
599 14th March and 27th March, where the storm occurred, are relatively mild ($H_s < 0.5$ m).

600

601

602 *Generating boundary forcings*

603

604 Hydrodynamic parameters (i.e. sea surface elevation and velocity fields) of the *Sefton*
605 area are simulated for the study period applying the Delft3D-FLOW module. The SWAN
606 model is used to simulate spectral wave parameters (i.e. H_s , T_p and *Direction*). Resulting
607 sea surface elevation and wave conditions are extracted at the offshore boundary of the
608 *Formby* domain to drive the high resolution *Formby* model setup in XBeach.

609

610

611 *Sensitivity analysis*

612

613 The XBeach model consists of a large number of model parameters. Morphological
 614 evolution is shown to be very sensitive to some of these parameters (McCall et al., 2010;
 615 Williams et al., 2011; Pender and Karunaratna, 2013). Therefore, a sensitivity analysis
 616 is carried out to tune a selection of model parameters, to be suitable for the Sefton coast.

617 The 1D model domain described in Section 4.1 is used to carry out the sensitivity
 618 analysis (see Figure 3) and simulations were carried out for the storm period described
 619 above (i.e. 27 March to 04 April 2010). Each selected parameter is systematically
 620 changed with reference to the base case which represents the factory settings of the
 621 XBeach model (Table 1). Altogether, there are 18 simulations undertaken in the
 622 sensitivity analysis.

623

Model parameter	Base simulation	Test No				Description
		1	2	3	4	
<i>wetslp</i>	0.3	0.15	0.60	-	-	avalanching occurs when defined slope exceeded
<i>smax</i>	1	0.8	1.2	-	-	Maximum Shield value for overwash/sheet flow condition
<i>form</i>	1	2	-	-	-	Define transport formula, 1-Soulsby-Van Rijn and 2-Van Thiesel-Van Rijn
<i>nuhv</i>	1	10	20	-	-	Additional shear dispersion factor to create advective mixing
<i>eps</i>	0.005	0.001	0.025	-	-	Threshold depth for drying and flooding
<i>morfac</i>	1	2	3	4	5	Morphological scale factor
<i>C</i>	57	30	90	-	-	Chézy coefficient
<i>facua</i>	0	0.5	1.0			Calibration factor for wave asymmetry transport

624

625

626

627 **Table 1 Model parameters and modified values in the 1D sensitivity simulations**

628

629

630 *2D area modelling*

631

632 The high resolution *Formby* domain is used to investigate the storm induced
633 morphological changes of the beach/dune system around Formby Point (i.e. the highly
634 dynamic area on the Sefton coast). Model parameters in XBeach are tuned based on the
635 sensitivity analysis described in section 4.4.2). The 2D simulation demands a large
636 computational power due to the extent of the model domain ($\sim 12 \text{ km} \times 15 \text{ km}$), high
637 grid resolution (min. $\sim 2 \text{ m} \times 25 \text{ m}$) and the morphological simulation period (8 days).
638 Therefore, the model runs are carried out on the Swansea University ‘Blue Ice’ HPC
639 Linux Cluster, which has 600 CPU-core and 1.2TB RAM processing capacity.

640

641

642

643

644

645 **5. Model results**

646 **5.1 Boundary forcings**

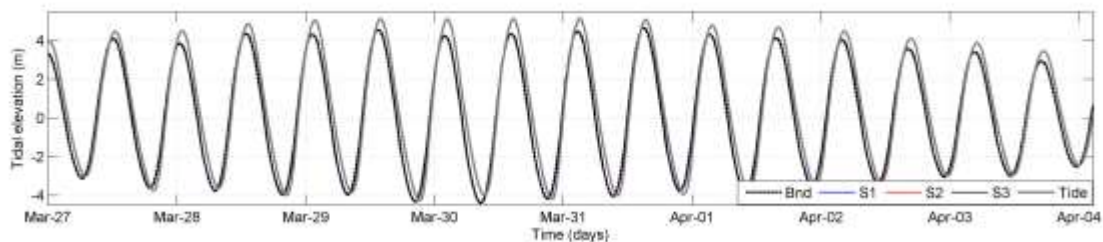
647

648 *Water level (WL)*

649

650 The total water elevation predicted by the Delft3D-FLOW module at the offshore
651 boundary of the *Formby* domain (*S1*, *S2* and *S3*, see Figure 5a) is shown in Figure 10.
652 The mean water elevation at the offshore boundary of the *Sefton* domain (*Bnd*) and the
653 observed tide (*Tide*) at the tide gauge (see *TG* in Figure 1) are also included in this figure
654 for comparison. In the *Sefton* model domain (i.e. cross-shore extent ~ 20 km), the
655 boundary water elevation is almost identical to that of the other locations; *S1*, *S2* and *S3*.
656 However, the observed elevation is slightly different to the boundary forcing and the
657 simulated elevation. The simulated elevation shows a better agreement during rising tide
658 than falling tide, implying a forward phase shift (i.e. lag behind the boundary tide). The
659 amplitude difference is higher at HW (max. ~ 0.8 m) than at LW. The tide gauge is
660 located inside the Mersey estuary, which is outside of our model domain. Therefore,
661 observed differences in phase and amplitude are expected due to the influence of local
662 bathymetry and geometric change to the propagating tidal wave (Dronkers, 2005; Wolf,
663 1981).

664



665

666 **Figure 10 Comparison of predicted tide at S1, S2 and S3 of the *Sefton* domain with the boundary**
667 **imposed tide (*Bnd*) and observed tide at the tide gauge (*Tide*) (see *TG* in Figure 1)**

668

669

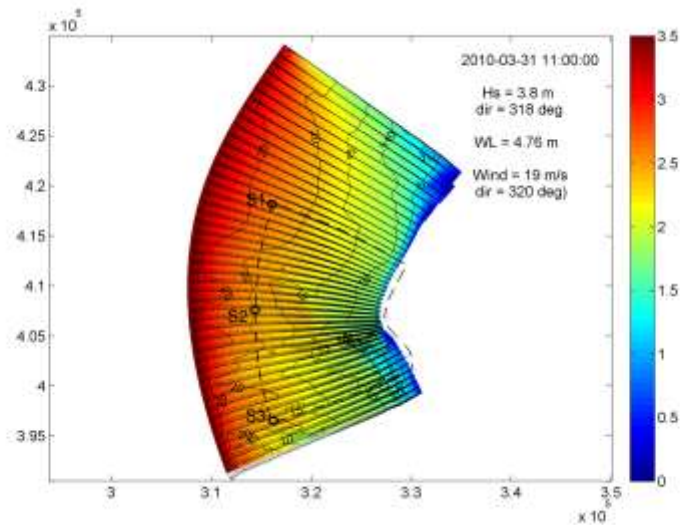
670 *Significant wave height (H_s)*

671

672 Evolution of the peak storm wave height (i.e. $H_s = 3.8$ m and dir. = 318^0 at 11:00 hours of
673 31st March 2010) for the SWAN simulation (see section 4.4), which occurs at HW (4.76
674 m ODN), is shown in Figure 11. The contours represent the total depth (MSL + HW
675 elevation) available for wave propagation at the peak of the storm. It can be seen that the
676 middle section of the Sefton coast (Formby Point and the surroundings) is exposed to
677 energetic wave conditions ($\sim 1.0 - 1.5$ m). The northern and southern parts are subjected
678 to fairly low wave conditions due to a very shallow foreshore with multiple bar-trough
679 systems towards the north and shielding from the Crosby channel towards the south
680 leading to a high degree of wave dissipation. The dash-outline shows the extent of the
681 *Formby* domain. The offshore points *S1*, *S2* and *S3* marked in the *Formby* domain are
682 used to compare and contrast the predicted wave transformation with the waves at the
683 offshore boundary of the *Sefton* domain.

684

685



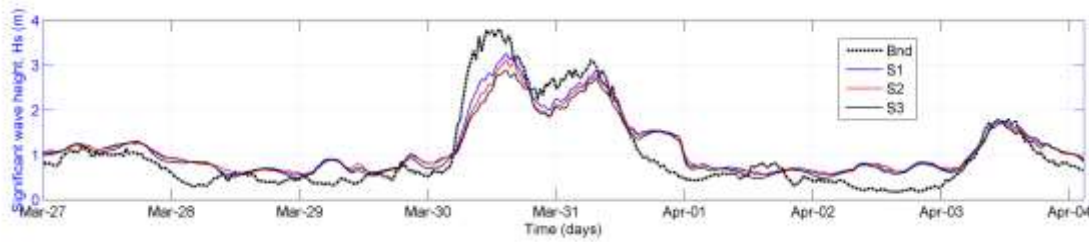
686

687 **Figure 11 Evolution of peak storm wave height across the *Sefton* model domain (Colour indicates**
 688 **magnitude of H_s ; Depth contours are drawn relative to the water surface; Dash-line shows outline of**
 689 **the *Formby* model and offshore boundary points $S1$, $S2$ and $S3$)**

690

691 Resulting waves (H_s , peak period (T_p) and direction) were extracted at offshore points
 692 ($S1$, $S2$ and $S3$) for comparison. The predicted H_s values at these locations are shown in
 693 Figure 12 with the boundary wave (Bnd) applied at the offshore boundary of the *Sefton*
 694 model (i.e. WaveNet data). Results indicate a general trend that higher waves (> 1 m)
 695 dissipate and lower waves (< 1 m) grow while propagating from offshore to nearshore
 696 areas. Along the offshore boundary of the *Formby* domain, the predicted wave heights
 697 decrease from North to South (i.e. from $S1$ to $S3$). This is mainly related to the sea bed
 698 bathymetry of this area where water depth decreases from $S1$ to $S3$. It should be noted
 699 that the increment of H_s from $S1$ to $S3$ is marginal at low wave conditions. The largest
 700 difference (~ 0.2 m) is found at the peak storm wave height.

701



702

703 **Figure 12 Boundary wave height of the *Sefton* model (Bnd) and transformed wave heights at the**
 704 ***Formby* model boundary; *S1*, *S2* and *S3* (see locations in Figure 11)**

705

706 Predicted wave conditions at *S2* are subsequently employed to represent the offshore
 707 wave boundary conditions of the *Formby* domain.

708

709

710 **5.2 Sensitivity analysis**

711

712 Evolution of the 1D profile (see Figure 3) applying the modified model parameters is
 713 compared with that of the base case (see Table 1). Results are analysed in terms of
 714 Cumulative Volume Change, change in the beach/dune interface and Root Mean Square
 715 Error.

716

717 Cumulative Volume Change (*CVC*) for a unit alongshore length at each morphological
 718 time step was estimated by multiplying depth change and grid cell distance along the
 719 profile. Resulting *CVC* values of all sensitivity tests are shown in Figure 13 for the 8 day
 720 storm duration (i.e. 27 March – 04 April). In the first three days, results of the base case
 721 show no volume change due to very calm wave action (i.e. offshore $H_s < 1$ m, see Figure

722 12). After about 3.5 days, *CVC* increases up to about 3 m³/m due to the first storm peak,
723 and thereafter another increase (~1 m³/m) occurs as a result of the second storm peak (see
724 Figure 12). It can be seen that the morphological change of the base case is proportional
725 to the magnitude of the storm peak wave height. This trend is found in all sensitivity test
726 cases except in ‘*morfac*’. A summary of sensitivity analysis is given below:

727

728 *wetslp*: Avalanching occurs when the defined critical slope (*wetslp*) is exceeded. Higher
729 slopes are expected to result in strong volume changes. In the present analysis, all
730 applications (0.15, 0.30 and 0.60) show similar *CVC* values (Figure 13a).

731

732 *smax*: This represents the maximum Shield criterion for overwash and sheet flow
733 conditions. Small values result in weak stirring and therefore less amount of sediment is
734 expected to release into the water column leading to weak volume change. After the
735 storm peak, *CVC* is proportional to the magnitude of *smax* (Figure 13b).

736

737 *form*: Sediment transport is estimated based on Soulsby-Van Rijn (1) or Van Thiesel-Van
738 Rijn (2) formulations. After the storm peak, (1) estimates marginally low *CVC* compared
739 with that of (2) (Figure 13c) due to inherent differences in both transport formulas (see
740 Van Thiel de Vries et al., 2008 and Soulsby, 1997).

741

742 *nuhv*: This is an additional shear dispersion factor to create an additional advective
743 mixing. Higher values increase the alongshore viscosity and then less amount of sediment

744 escapes into the water column. A marginal difference of *CVC* is observed after the storm
745 peak (Figure 13d) which indicates the highest volume change applying the lowest value.
746

747 *eps*: Threshold depth for the drying and flooding algorithm is defined by *eps*. Small *eps*
748 results in many wet grid cells, contributing to hydrodynamics and therefore increase in
749 sediment transport compared to that of a large value. Sensitivity tests indicate similar
750 *CVC* values under all three values (Figure 13e).
751

752 *morfac*: Application of the *morfac* value accelerates the bed level changes while
753 decreasing the simulation period (Roelvink, 2006; Lesser et al., 2004). Systematic
754 analysis of *morfac* selection is always recommended before applying a *morfac* value to
755 investigate morphological changes (Dissanayake et al., 2009; 2012; Dissanayake and
756 Wurpts, 2013). In the case of *morfac* tests, it was found that the bed evolution is mainly
757 dominated by *morfac* value rather than the storm action. *morfac* = 1 shows relatively
758 constant change (i.e. max. < 4 m³/m). Application of 2 and 3 results in *CVC* more than 20
759 m³/m while 4 and 5 show about 10 and -10 m³/m volume change respectively at the end
760 of the 8 day period. These results indicate that it is not realistic to apply higher *morfac*
761 value (> 1) to accelerate the morphological evolution (i.e. to decrease the computational
762 period) in the present analysis.
763

764 *C*: Smaller the Chézy coefficient the higher the bed roughness value imposing lower
765 sediment transport rates. Our analysis shows, *C* = 30 has no positive change in *CVC*
766 during the storm action due to very strong bed roughness compared to the cases of 57 and

767 90 (Figure 13g). The lowest bed roughness ($C=90$) results in the highest $CVC (> 10$
 768 m^3/m).

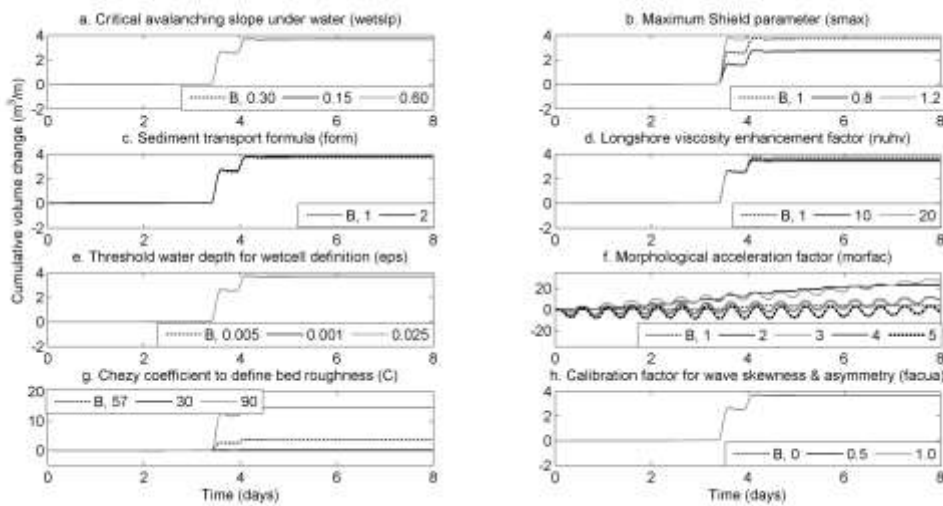
769

770 *facua*: This parameter determines the contribution of wave asymmetry into the sediment
 771 transport. Sensitivity tests were undertaken applying no contribution (0), partial
 772 contribution (0.5) and fully contribution (1). However, they present almost similar CVC
 773 during the evolution (Figure 13h) implying that the wave asymmetry contribution on
 774 sediment transport is marginal in the situation considered in the present study.

775

776

777

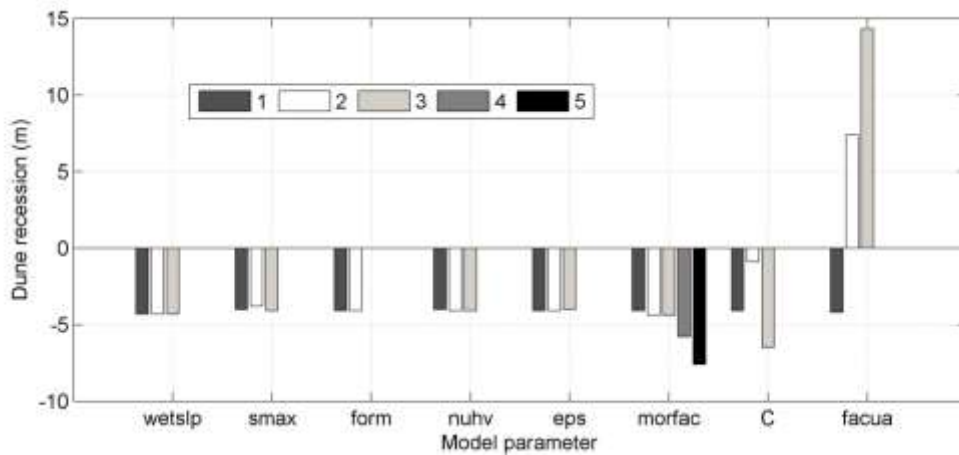


778

779 **Figure 13 Cumulative Volume Change (CVC) (m^3/m) of the cross-shore profile (P14, see in Figure 3)**
 780 **in the Base case run and sensitivity runs (see Table 1 for Model parameters and modified values in**
 781 **the 1D sensitivity simulations)**

782

783 Storm impacts on the beach/dune interface evolution are of special interest for the coastal
 784 managers in order to apply mitigation measures. In our sensitivity analysis, cross-shore
 785 variation of the beach/dune interface was estimated based on the 4.4 m ODN level. If
 786 water level reaches this threshold (note. tidal level exceeds 4.7 m ODN in the selected
 787 storm), a few meters of dune recession is expected under moderate waves within a single
 788 tide (Pye and Blott, 2008). Resulting dune recession values are shown in Figure 14
 789 corresponding to the each sensitivity run. It is generally found that the model predicts
 790 about 4 m of dune recession, though some cases resulted in accretion at the beach/dune
 791 interface (see last two in '*facua*'). This provides a qualitative impression of the amount of
 792 the dune recession within the selected storm event.
 793



794
 795 **Figure 14** Change in the representative dune toe level (4.4 m ODN, Pye and Blott, 2008) in the cross-
 796 shore direction during the sensitivity runs with respect to the base case (see Table 1). Legend shows
 797 the test cases undertaken.
 798

799
 800 CVC and dune recession analyses provide relative impact of each coefficient and wave
 801 action on the beach/dune evolution along the storm duration. However, it is difficult to

802 determine the suitable coefficients for the study area based on the *CVC* alone, as the
803 measured profile length covers only a part of the simulated profile. Therefore, the Root
804 Mean Square Error (*RMSE*) between the simulated and measured profiles was also
805 calculated. In contrast to the *CVC* analysis, *RMSE* uses a portion of the simulated profile
806 (i.e. enclosing dune and beach areas) based on the measured profile length. *RMSE* is
807 given by *Eq 1* considering the changes at each grid cell of the selected profile length.

808

809

$$RMSE = \sqrt{\frac{\sum(z_{measured} - z_{predicted})^2}{N}}$$

810 (1)

811

812 where; $z_{measured}$, measured post-storm profile depth; $z_{predicted}$, predicted post-storm profile
813 depth and N , number of grid cells. The lower the *RMSE* the higher the agreement
814 between measured and predicted profiles.

815

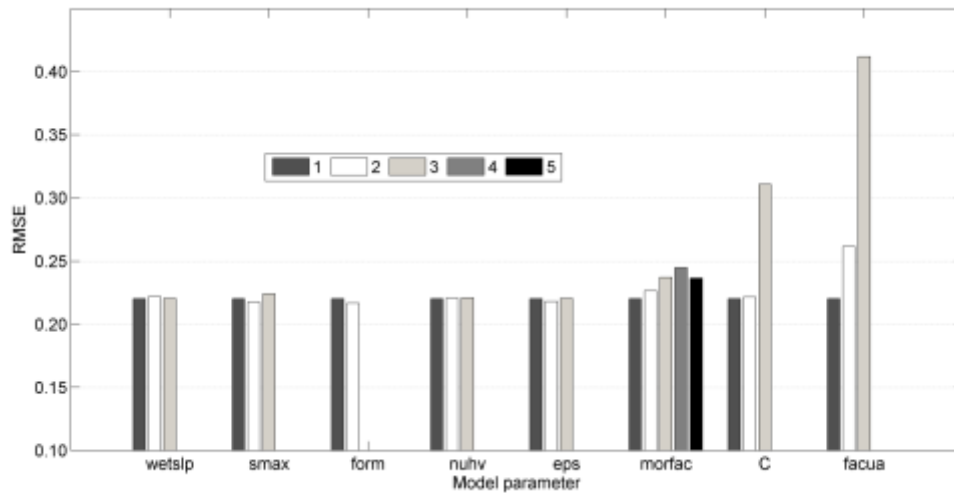
816 Computed *RMSE* values are shown in Figure 15 for the base case and the different test
817 cases carried out. The sequence of bars is referred to the test number in Table 1. Each
818 cluster of bars represents the sensitivity of bed evolution to the modified values of the
819 respective coefficients.

820

821 The change of first five coefficients (*wetslp*, *smax*, *form*, *nuhv* and *eps*) induced a
822 marginal difference of the *RMSE*, which implies the fact that the sea bed evolution is not

823 significantly sensitive to these parameters. The last three clusters (*morfac*, *C* and *facua*)
 824 give relatively higher variability in *RMSE* indicating that the profile change is more
 825 sensitive to these model parameters than the others. The optimal value for each
 826 coefficient, which gives the lowest *RMSE* (see bold figures in each test case in Table 1)
 827 was selected for the 2D simulations given in Section 5.3. Accordingly, *smax* and *form*
 828 require adjusted values while all others remain as the default settings, which were
 829 implemented in the base case simulation.

830



831

832 **Figure 15 Estimated *RMSE* of sensitivity runs with respect to the Base case. Legend shows test cases**
 833 **undertaken in each parameter**

834

835

836

837 **5.3 Evolution of the beach/dune system**

838

839 *Application of the morfac value*

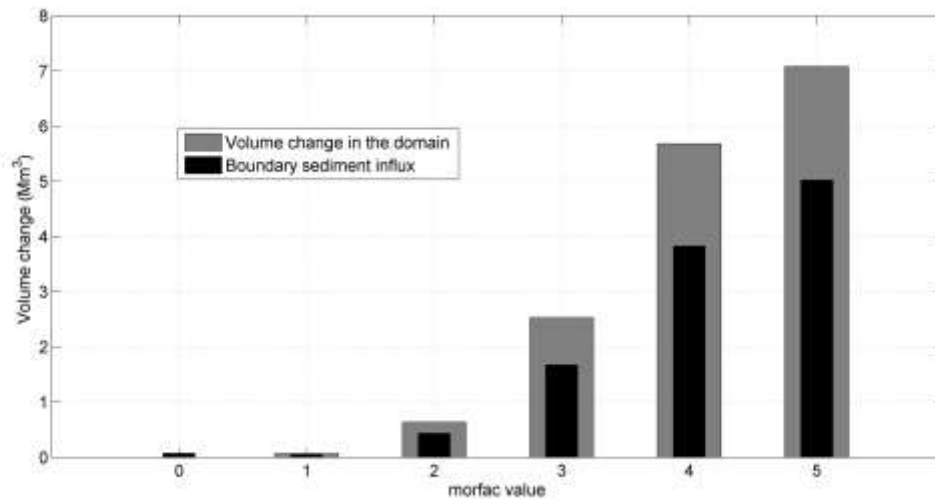
840

841 A 2D morphodynamic simulation in the *Formby* domain requires about 1.6 days of a
842 computational time on the HPC Linux cluster due to the finer grid resolution and the
843 length of the morphological period (from 27 March to 04 April 2010). Therefore,
844 potential application of the *morfac* value was further investigated. 2D morphodynamic
845 simulations were carried out for the entire storm duration using *morfac* values of 1, 2, 3,
846 4 and 5). In addition, the *morfac* = 0 case (i.e. no morphological changes) was
847 investigated to estimate the sediment influx into the model domain from the open
848 boundaries.

849

850 Volume change of the model domain during the morphological period was estimated by
851 multiplying bed level change of each grid cell by the area of the cell. Positive volume
852 change implies sediment gain while negative change shows sediment loss from the
853 system. In the simulations, all three open boundaries (i.e. north, south and west see in
854 Figure 5) were set to have equilibrium sediment concentration (Galappatti, 1983) which
855 allows sediment input/output based on the estimated concentration during the evolution.
856 At each time step, the boundary sediment supply was computed by using the increment in
857 grid cell size, to represent the distance along the boundary, multiplied by the
858 corresponding sediment component perpendicular to the boundary. Then, the total
859 sediment supply was calculated by as the sum over all time-steps. The estimated volume
860 change and boundary sediment supply are shown in Figure 16 for all *morfac* applications.

861



862

863 **Figure 16 Comparison of mass-conservation with different *morfac* applications; Volume change in**
 864 **the model domain (grey) and Boundary sediment input into the domain (black)**

865

866 They indicate sediment is being received into the system; a positive boundary input. It
 867 should be noted that the volume increase in the domain should be equal to the boundary
 868 sediment input in order to satisfy the mass conservation during the morphodynamic
 869 evolution.

870

871 The *morfac* = 0 case shows the boundary sediment influx into the model domain,
 872 indicating that the domain receives sediment from outside. For all non-zero *morfac*
 873 applications, volume change is not equal to the boundary sediment influx, which indicate
 874 mass conservation is not fulfilled. The lowest difference between volume change and
 875 boundary sediment influx (0.02 Mm³) is found when *morfac*=1 is used and the highest (2
 876 Mm³) for *morfac*=5. It may be argued that the smallest difference (0.02 Mm³) may occur
 877 as a result of errors arising from average depth considerations of a grid cell in the
 878 estimation of the volume change and therefore, considered as acceptable. The differences

879 between boundary sediment influx and volume change in the domain is significantly
880 large and is unacceptable for the *morfac* > 1 cases. Additionally, the erosion and
881 sedimentation patterns show unacceptably large changes along the dune front and at the
882 offshore boundary (not shown) as the *morfac* increases. Therefore, we use *morfac*=1 for
883 all simulations herein.

884

885

886 *Erosion and sedimentation pattern*

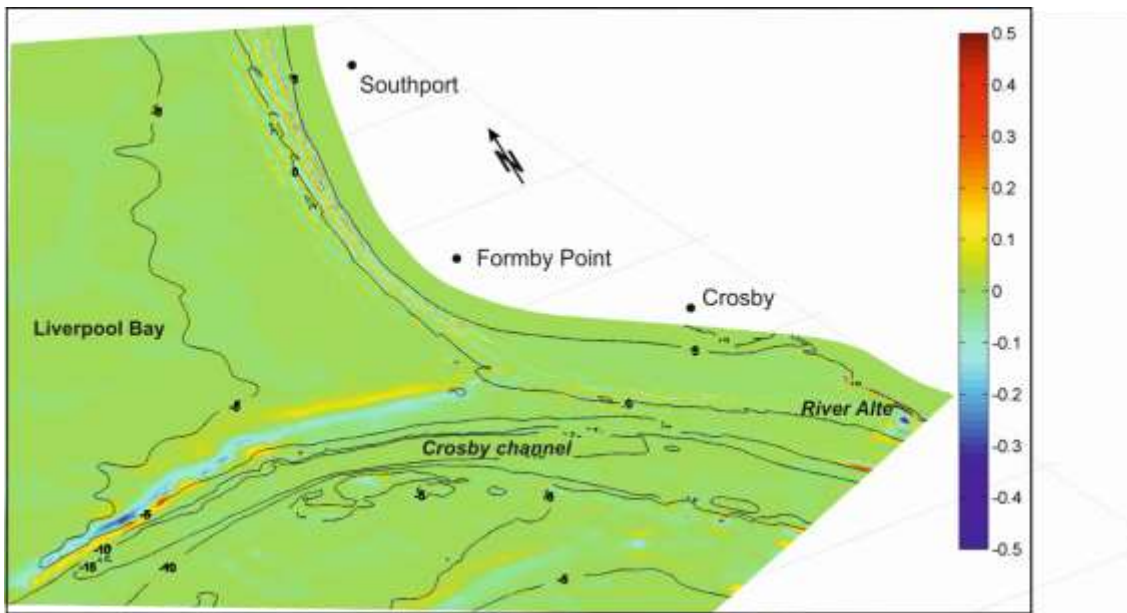
887

888 Morphological change in the *Formby* domain from the 27th March to 04th April 2010 is
889 shown in Figure 17. Initial depth contours at 5 m intervals are also shown in the same
890 figure for clarity. Significant bed level changes in the range of – 0.5 m (erosion) to 0.5 m
891 (deposition) are found mainly in two areas of the domain; 1) beach/dune system between
892 Southport and Formby Point and 2) north of the Crosby channel. These patterns provide a
893 qualitative indication of the interaction between storm driven hydrodynamic forces and
894 the bed morphology.

895

896 The strongest bed level changes seem to appear along the coastal stretch between
897 Southport and Formby Point. According to the direction of the peak storm wave height
898 (NW) and the orientation of the Sefton coast, it is evident that this area is more
899 susceptible to the wave action. The maximum recorded WL of this storm is about 4.8 m
900 ODN which could result in soaking of the dune foot and wave under cutting at the
901 proximity of +5 m contour (see erosion patches adjacent to this contour in Figure 17).

902 This is more pronounced at north compared with that at south of this stretch because the
903 beach/dune system at north is exposed to stronger waves (see Figure 11 during peak storm
904 wave height). Bed evolution indicates alternate areas of erosion and sedimentation (i.e.
905 forming runnels and ridges respectively) which are almost aligned with the initial depth
906 contours. These are typical morphological features found after a storm attack on a sandy
907 beach/dune system (Roelvink et al., 2009; Plater and Grenville, 2010). The significance
908 of these features gradually decreases from the dune front towards the offshore, indicating
909 strong morphological evolution of the dune front.
910
911



912
913 **Figure 17 Erosion (blue) and Sedimentation (red) during the March 2010 storm event (from 27**
914 **March to 04 April). Contours indicate the initial bed topography**
915
916 The seaward extension of the 5 m depth contour along the north bank of the Crosby
917 channel implies a sand ridge on the initial bed topography. Such a shoal area interrupts

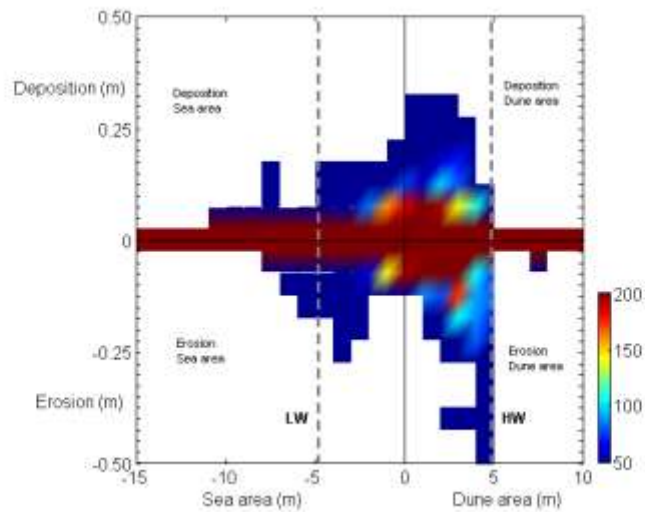
918 the NW incoming waves, which can lead to strong wave breaking in that area. This
919 process may result in large bed level changes in the neighbouring areas. The eroding area
920 is aligned with the ridge, which shows maximum wave interaction and dissipation
921 occurring at highest bed levels. The highest erosion is found at the seaward end of the
922 ridge and the eroded sediment has subsequently deposited at the leeward side. However,
923 at the proximity of MWL, weak erosion is found at leeward side of the ridge and
924 deposition is at the windward side. This may be due to the tidal currents enhanced by the
925 presence of the Crosby channel (Thomas et al., 2001). Therefore, the predicted
926 erosion/sedimentation patterns provide a qualitative impression on which areas are more
927 prone to storm impacted bed level changes along the Sefton coast.

928

929

930 Bed level changes are further analysed in order to find areas of weak and strong depth
931 variations. Density of erosion and deposition points with respect to the depth contours
932 indicates the significance of bed level change in different regions of the domain (see
933 Figure 18). The depth contours from 0 to 10 m represent the dune area while 0 to -15 m
934 represent the sea area (see x axis). The y axis shows the bed changes (erosion – negative
935 and deposition – positive). Two-vertical dashed-lines mark LW and HW limits (i.e. inter-
936 tidal range).

937



938

939 **Figure 18 Density of erosion and deposition points with the depth contours (see colour bar); LW and**
 940 **HW indicate inter-tidal range in the domain; x axis shows depth contours while y axis indicates bed**
 941 **level change.**

942

943 Four quadrants in Figure 18 show deposition/dune area, erosion/dune area, erosion/sea
 944 area and deposition/sea area. The highest density of bed level changes (> 200) is found in
 945 the range of -0.025 to 0.025 m from the dune area to sea area (see around $y = 0$). The
 946 intertidal region shows the most bed evolution in the domain. The area above MWL has
 947 greatest erosion (~ -0.5 m) and deposition (~ 0.3 m). The greatest erosion occurs at the
 948 dune front (i.e. see around 5 m contour). Density variation indicates that the eroded
 949 sediment has been transported towards MWL as found with the alternate erosion and
 950 sedimentation areas in Figure 17. The strongest deposition is shown in between 0 and 3 m
 951 contour levels. Below MWL, there are some areas which are subjected to relatively high
 952 erosion and deposition and they may be related to the locations of sand ridges in the
 953 initial sea bed.

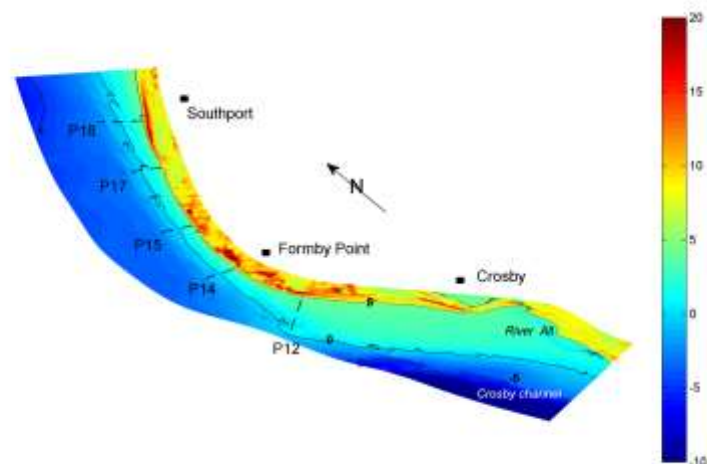
954

955

956 *Profile evolution*

957 Post-storm profile measurements have been carried out on the 04th April 2010 (Williams
958 et al., 2011). These survey data cover the upper beach profile of the Sefton coast from
959 about 0.5 m ODN to the dune frontage. Five representative profile locations were used in
960 order to compare the measured and predicted storm induced bed evolution. These profiles
961 are shown on the beach/dune topography of the model domain (note. part of the Formby
962 model domain is present in Figure 19 for clarity). The 5 m depth contour demarcates
963 beach and dune area. The first three profiles (P12, P14 and P15) present the highly
964 dynamic area of the Formby Point which has the highest dune crests (max. height > 20 m
965 ODN). P12 and P14 run through these higher dune areas (> 15 m ODN) while P15 has a
966 relatively low dune height (< 15 m ODN). At P17, the profile indicates the lowest dune
967 crest height (< 10 m ODN). At the north of the dune system, there is a linear dune row
968 (max. height ~ 20 m ODN) parallel to the 5 m depth contour. The fifth profile, P18, is
969 located across this dune row.

970



971

972 **Figure 19 Selected profile locations (P12, P14, P15, P17 and P18) to compare measured and predicted**
973 **bed evolution. Beach/dune system is shown with the depth contours (-5, 0 and 5 m ODN) and the**
974 **topography (see colour bar).**

975

976 Initially, the model predicted evolution at the selected profile locations was analysed with
977 respect to the initial model bathymetry. As discussed in the 1D sensitivity runs, change in
978 the beach/dune interface (i.e. dune recession) was estimated based on the 4.4 m ODN
979 level (see Table 2). The highest dune recession is at P17 where there are lower dune
980 heights, while the lowest recession is found at P12 with higher dune areas. These
981 predictions agree with Edelman (1968) who concluded that the dune recession is
982 inversely related to the dune height. This indicates that the lower dune areas are
983 susceptible to storm impacts and need more focus in implementing management
984 strategies. Extent of cross-shore bed level change was estimated using the distance
985 between the beach/dune interface and the seaward depth at which marginal changes are
986 expected beyond this point. At Formby Point, cross-shore sediment fluxes extend to
987 longer seaward distances (see P14 and P15) implying strong bed evolution compared
988 with other locations. These results indicate that analytically derived closure depth value
989 (< 15 m, see section 4.1) is not applicable to the entire coast and the profile P15 is highly
990 influenced (i.e. largest closure depth) by the alongshore sediment transport from Formby
991 Point. These processes are further evident from the cross-shore volume changes along the
992 Sefton coast (i.e. strongest negative volume change (erosion) is at the latter two profiles).
993 It should be noted that using our 2D simulations, a similar analysis can be carried out for
994 the entire Sefton coast. Results for a few selected cross shore locations are given in Table
995 2.

996

997

998

Profile No	Change in beach/dune interface (4.4 m ODN level) in cross-shore direction (m)	Extent of cross-shore changes		Cross-shore volume change (m ³ /m)
		Closure distance from the 4.4 m ODN level (km)	Closure depth (m ODN)	
P12	-0.5	3.0	-8.6	-11.4
P14	-2.0	8.9	-10.1	-15.8
P15	-1.6	10.4	-10.3	-15.8
P17	-3.6	0.6	-3.0	-10.3
P18	-1.6	2.0	-5.6	-13.1

999

1000

1001

1002

1003

Table 2 Model predicted bed evolution at the selected profile locations with respect to cross-shore change of the beach/dune interface (4.4 m ODN level, Pye and Blott, 2008) (negative change is dune recession), cross-shore extent of bed level change and volume change for unit alongshore length (negative change is erosion).

1004

1005

Predicted morphological changes of these profiles were extracted from bed level changes

1006

in the 2D bed evolution simulations at the same locations of measured profile

1007

coordinates. The resulting profile evolutions during the storm period (i.e. initial and final

1008

predicted profiles) are shown in Figure 20 with the measured post-storm profiles. It is

1009

noted that the measured profiles cover only a part of the complete profile and only for the

1010

post-storm conditions. A comparison of measured and simulated profiles at these

1011

locations is given below:

1012

1013

1014

a. Profile P12

1015

Evolution of *P12* during March - April 2010 storm is shown in Figure 20a. This profile

1016

has a very gentle slope (>1:100) below the dune foot and indicates marginal changes

1017 during the storm event. A good agreement between simulated and measured post-storm
1018 profiles can be seen, except at elevations higher than 5.5 m ODN. It should be noted that
1019 the measured profile segment spans from about 80 m to 230 m in seaward distance.

1020

1021

1022 *b. Profile 14*

1023

1024 *P14* has a very steep dune face (Figure 20b). Predicted results show a slight beach
1025 lowering at the dune foot and between 200 - 230 m cross shore distance. The measured
1026 profile spans from 100 m to 250 m. The predicted and measured post-storm profiles show
1027 an encouraging agreement.

1028

1029

1030 *c. Profile 15*

1031

1032 Profile shape of the 2D model bed has ridge and runnel variations (see black-dash-line in
1033 Figure 20c). Predicted results show areas of erosion and accretion along the profile
1034 during the storms. Measured post storm profile segment spans about 100 m (from 175 m
1035 to 275 m) from 2.5 m ODN to 0.5 m ODN in elevation. The measured post-storm profile
1036 shows lower beach levels than the predicted levels.

1037

1038

1039 *d. Profile 17*

1040

1041 The lowest dune crest height (< 10 m ODN) is found in *P17* (Figure 20d) compared with
1042 the other profiles. Measured post-storm profile segment has a length of about 160 m
1043 (from 90 m to 250 m). The predicted post-storm profile agrees well with the measured
1044 profile except between 130 m and 190 m chainages.

1045

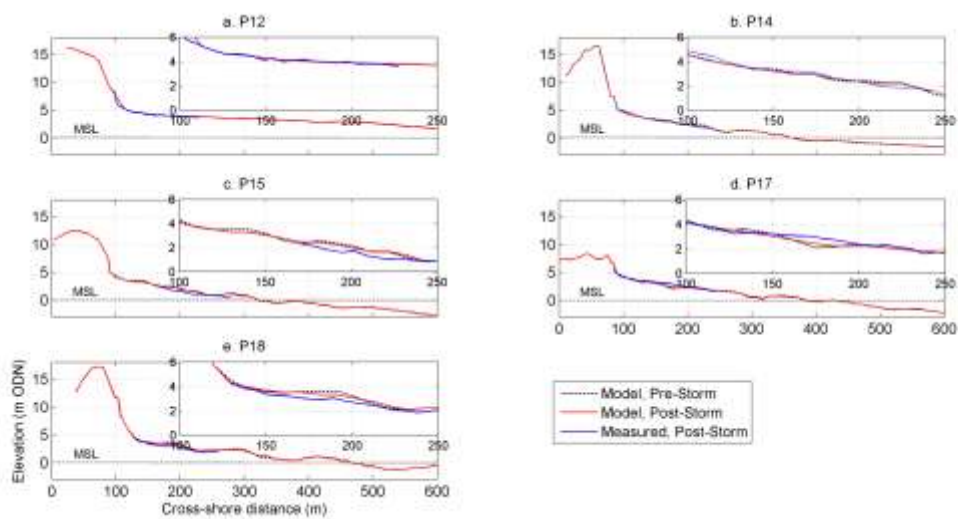
1046

1047 *e. Profile 18*

1048

1049 The highest dune elevation (17.2 m ODN) is found in *P18* (Figure 20e). The profile has
1050 three bars and troughs from 120 m to 600 m. Predicted results show erosion of the bars
1051 and deposition at the troughs. Measured post-storm profile extends from about 120 m to
1052 260 m, covering a single bar and a trough. The predicted and measured post-storm
1053 profiles agree reasonably well except in an area around the crest of the profile.

1054



1055

1056 **Figure 20 Comparison of measured and model predicted cross-shore profiles; P12, P14, P15, P17 and**
 1057 **P18 (see locations in Figure 19); Model pre-storm (black-dash-line), Model post-storm (red-line) and**
 1058 **Measured post-storm (blue-line)**

1059

1060 To quantify the comparison of predicted and measured post-storm cross shore profiles,
 1061 three statistical parameters, *RMSE*, Brier Skill Score (*BSS*) and Correlation coefficient
 1062 (R^2) are used.

1063

1064 Averaged *RMSE* value was estimated as discussed in section 5.2. The lower the *RMSE*,
 1065 the higher the agreement between predicted and measured profiles. Resulting *RMSE*
 1066 values for each profile prediction are given in Table 3. The lowest *RMSE* (0.19) is found
 1067 in the *P14* while the highest (0.39) is in the *P15*, implying that the *P14* and *P15* provide
 1068 the best and the worst predictions respectively compared to the measured post-storm data.
 1069 Both *P12* and *P17* result in *RMSE* of 0.34. The *P18* gives a *RMSE* of 0.29.

1070

	Profile No				
Parameter	12	14	15	17	18
RMSE	0.34	0.19	0.39	0.34	0.29
BSS	0.88	0.96	0.84	0.87	0.90
R2	0.90	0.98	0.48	0.89	0.83

1071 **Table 3 Statistical comparison of measured and model predicted profiles (P12, P14, P15, P17 and**
 1072 **P18) using *RMSE*, *BSS* and R^2**

1073

1074 The *BSS* definition is given in *Eq. 2* (Van Rijn et al., 2003). Van Rijn et al (2003) have
 1075 classified the model predicted bed evolution according to the resulting *BSS* value (e.g. 0 –
 1076 0.3 *Poor*; 0.3 – 0.6 *Reasonable/Fair*; 0.6 – 0.8 *Good*; 0.8 – 1.0 *Excellent*).

1077

$$1078 \quad BSS = 1 - \frac{\langle (z_{measured,post-storm} - z_{model,post-storm})^2 \rangle}{\langle (z_{measured,pre-storm} - z_{model,post-storm})^2 \rangle}$$

1079

(2)

1080

1081 where, $z_{measured, post-storm}$, measured profile elevation after the storm; $z_{measured, pre-storm}$,

1082 measured profile elevation before the storm (i.e. initial model bed in the present

1083 analysis); $z_{model, post-storm}$, model predicted final profile elevations after the storm.

1084

1085 Resulting *BSS* values show the highest (0.96) in *P14* and the lowest (0.84) in *P15* while

1086 *P12* and *P17* have almost similar values (~0.88). *P18* has a *BSS* of 0.90. Therefore, the

1087 trend of *BSS* variation in each profile is similar to that of the *RMSE* values. According to

1088 Van Rijn et al (2003) classification, model simulations at all profiles qualify as

1089 'Excellent'.

1090

1091 The third statistical parameter used in this analysis is Correlation coefficient which is

1092 defined in *Eq. 3*. Higher R^2 values imply high degree of similarity between measured and

1093 model predicted profiles.

1094

1095

$$R^2 = 1 - \frac{\sum (z_{measured,post-storm} - z_{model,post-storm})^2}{\sum (z_{measured,post-storm} - \langle z_{measured,post-storm} \rangle)^2}$$

1096

(3)

1097

1098 The highest (0.98) and the lowest (0.48) R^2 values are found in *P14* and *P15* respectively
1099 R^2 values at *P12* and *P17* are almost identical (~0.90). R^2 value at *P18* is 0.83.

1100

1101 Even though statistical measures such as *RMSE*, *BSS* and R^2 gave very encouraging
1102 results for comparison of predicted profiles with the measured data, there are some
1103 discrepancies between the profiles. These can be attributed to two main reasons: slight
1104 mismatch of predicted and measured profile locations as measured profile information
1105 did not include coordinates; differences in profile resolution- predicted results are at a
1106 much higher resolution than the measured data.

1107

1108

1109 **6. Discussion**

1110 The LiDAR data (i.e. used to construct pre-storm bathymetry) and the observed post-
1111 storm profile data had different horizontal and vertical resolutions. This and some
1112 uncertainties regarding the accuracy of measurements may have caused some
1113 inaccuracies in the model predictions. This research, which is still continuing, is working
1114 alongside coastal managers, highlighting the observational needs for more detailed model
1115 validation; while understanding the model outputs required to advise regional monitoring
1116 schemes to maximise the usage of data collection for both management and research
1117 purposes. The aim is to ensuring science research is of benefit to coastal management
1118 addressing the gaps in knowledge.

1119

1120 To enable the longer term modelling, selection of the morfac value is required and is an
1121 entirely site specific process which depends on the local morphological and boundary
1122 forcing characteristics. Therefore, a sensitivity of bed evolution to morfac value should
1123 always be investigated prior to the selection of an optimum value for a given case study
1124 (Dissanayake et al., 2009; 2012; Dissanayake and Wurpts, 2013; Roelvink, 2006).

1125 Following this hypothesis, we systematically tested incremental morfac values (i.e. 1, 2,
1126 3, 4 and 5) to find the most suitable value for the current application.

1127

1128 Present study is a part of an on-going 3-year research project in which the main focus is
1129 to investigate the impacts of storm clusters on the evolution of Sefton beach/dune system.

1130 The model setup used in this study will then be extended to investigate the beach profile
1131 response to storm sequences, in order to identify the contribution of storms on the long-
1132 term dune change.

1133

1134 The initial research presented suggests the northern part of the Sefton coast incurred
1135 stronger morphological changes than the southern part due to the direct exposure to NW
1136 peak storm waves of the selected storm. Resulting bed evolution of the beach/dune
1137 system indicated an alternate pattern of erosion and accretion areas, which is shown to be
1138 typical of the study area (Plater and Grenville, 2010). The shoal area located to the north
1139 of the Crosby Channel obstructs NW waves resulting relatively calm wave action on the
1140 southern part of the Sefton coast. As a result, morphological changes along the Crosby
1141 channel and on the adjacent dune system is significantly low.

1142

1143 Sediment exchange volumes between dune face and beach foreshore were quantified at
1144 selected cross-shore profile locations. This is useful to identify erosion prone areas along
1145 the Sefton coast. Further, the closure distance and depth were estimated based on the
1146 model predicted evolution which shows how far eroded material move seaward. It was
1147 evident that the beach/dune system of the Sefton coast has very complex spatial
1148 variability.

1149

1150 This study further provides important messages for the XBeach model user community.
1151 In addition to the dune system along the upper beach the lower beach of the Sefton coast
1152 consists of a complex ridge-runnel system, most likely due to the hyper tidal conditions.
1153 Present application shows the ability of the model to capture not only the
1154 morphodynamic variability of the upper beach but also the ridge-runnel system and the
1155 models ability to perform under such large tidal regimes. Most previously recorded
1156 XBeach applications were limited to straight line coastal systems. Here we demonstrated
1157 the ability of the model in capturing morphodynamics of a convex coastline, which
1158 confirms models ability to capture dynamics of diverse coastal system.

1159

1160

1161

1162 **7. Conclusions**

1163

1164 A numerical model study was carried out in order to hindcast the storm-induced dune
1165 evolution at the Sefton coast in the Liverpool Bay, UK, using a storm event that occurred

1166 during March-April 2010. A nested modelling approach was used by combining a coarser
1167 model domain to transform offshore hydrodynamics (i.e. tides, surge and waves) up to
1168 the nearshore area and a fine-grid model to investigate the morphological evolution.
1169 Predicted bed evolution was analysed and compared with measured post-storm profiles
1170 available at a number of cross-shore locations along the beach in order to enhance the
1171 understanding of the potential storm impact on the Sefton beach/dune system. Results
1172 suggest following conclusions:

1173

1174 • Compared with many coastal locations, the Sefton coast has a rich set of
1175 information on tides, waves and morphological changes. However, if sediment
1176 transport data were also available, a better model calibration could have been
1177 done. Also, it should be noted that the storm event used in this study was not one
1178 of the extreme storms occurred in this region. However, we were restricted to use
1179 this storm at this instant due to limited availability of post-storm profile
1180 measurements for other larger storms.

1181

1182 • Wave model results indicate a general trend that higher waves (> 1 m) dissipate
1183 and lower waves (< 1 m) grow while propagating from offshore to nearshore
1184 areas.

1185

1186 • Morphological updating facility *morfac* available in the XBeach model (*morfac* >
1187 1 approach) was not suitable to the prevailing environmental conditions of the
1188 Sefton coast (i.e. a hyper-tidal region).

- 1189
- 1190 • Resolution of the observed data (LiDAR data and post-storm profiles) and the
- 1191 uncertainties therein may have underestimated the model predicted bed evolution
- 1192 to some extent.
- 1193
- 1194 • H_s of the March 2010 storm shows a double-peak of which the maximum
- 1195 occurred on the 31st March due to higher wave and wind conditions approaching
- 1196 from WNW sector during rising tide, which resulted the greatest bed evolution on
- 1197 the Sefton beach/dune system.
- 1198
- 1199 • Comparison of pre- and post-storm dune-beach profiles at five cross-shore
- 1200 locations along the beach show that a small amount of dune face erosion occurred
- 1201 during the storm. However, it should be noted that the selected storm (max. H_s =
- 1202 3.8 m) is not significantly severe compared with large storms that occur in this
- 1203 region ($H_s \sim 4$ m for 1 in 1 year event).
- 1204
- 1205 • Statistical comparisons (i.e. $RMSE$, BSS , R^2) suggested good agreement between
- 1206 predicted and measured post-storm profiles thus reassuring that the selected
- 1207 modelling approach is capable of satisfactorily predicting the morphodynamic
- 1208 evolution at the Sefton coast.
- 1209
- 1210 • Results on dune recession, cross-shore/alongshore variability of morphological
- 1211 changes and depth of closure values and distances of influence along the Sefton
- 1212 coast in the storm event scale provide useful qualitative information for coastal

1213 managers, to update/revise conceptual maps of sediment fluxes that are used in
1214 current shoreline management practise.

- 1215 • Results show the XBeach model’s ability to simulate the complex ridge-runnel
1216 system of the lower beach in addition to the dune erosion along the upper beach in
1217 a hyper-tidal environment (i.e. spring-tidal range > 8 m).
- 1218 • We demonstrated the potential application of the XBeach model for a complex
1219 coastal system (i.e. 2D convex coastline) though the model was initially
1220 developed for straight line coasts.

1221
1222
1223
1224
1225 The present model study provides preliminary insights to the storm-induced
1226 morphodynamics of the Sefton coast dune system. These findings will have important
1227 implications on interpretation of the observed dune erosion at the Sefton coast and will be
1228 useful in formulating sustainable dune management strategies. On-going study extends
1229 this morphological model setup to estimate potential wave overtopping and flood risks
1230 during future single storm events and storm clusters.

1231

1232 **Acknowledgements**

1233 The work presented in this paper was carried out under the project ‘FloodMEMORY
1234 (Multi-Event Modelling Of Risk and recoverY)’ funded by the Engineering and Physical
1235 Sciences Research Council (EPSRC) under the grant number: EP/K013513/1. Prof. John

1236 Williams is greatly acknowledged for providing post-storm profile data, collected as part
1237 of the MICORE project (EU FP7 program Grant 202798). BODC, NTSLF and CEFAS
1238 (WaveNet) are acknowledged for providing tidal and wave data respectively. Sefton
1239 Metropolitan Borough Council is appreciated for the access of other relevant data used in
1240 this study.

1241

1242

1243 **References**

1244 Blott, S.J., Pye, K., Van der Wal, D., Neal, A., 2006. Long-term morphological change and its causes in the
1245 Mersey Estuary, NW England, *Geomorphology* 81, 185 – 206.

1246

1247 Booij, N., Ris, R.C., Holthuijsen, L.H., 1999. A third generation wave model for coastal regions, Part I,
1248 Model description and validation, *Journal of Geophysical Research* 104, C4, 7649 – 7666.

1249

1250 Bosboom, J., Aarninkhof, S.G.J., Reniers, A.J.H.M., Roelvink, J.A., Walstra, D.J.R., 2000. UNIBEST-TC
1251 2.0 – overview of model formulations. Rep, H2305.42, Delft Hydraulics, Delft.

1252

1253 Bricheno, L.M., Wolf, J.M., Brown, J.M., *in press*. Impacts of high resolution model downscaling in
1254 coastal regions, *Continental Shelf Research*.

1255

1256 Brown, J.M., 2010. A case study of combined wave and water levels under storm conditions using WAM
1257 and SWAN in a shallow water application, *Ocean Modelling* 35, 215 – 229.

1258

1259 Brown, J.M., Souza, A.J., Wolf, J., 2010a. An investigation of recent decadal-scale storm events in the
1260 eastern Irish Sea, *Journal of Geophysical Research* 115, C05018, doi: 10.1029/2009JC005662.
1261

1262 Brown, J.M., Souza, A.J., Wolf, J., 2010b. An 11-year validation of wave-surge modelling in the Irish Sea,
1263 using a nested POLCOMS-WAM modelling system, *Ocean Modelling* 33, 118 – 128.
1264

1265 Brown, J.M., Souza, A.J., Wolf, J., 2010c. Surge modelling in the eastern Irish Sea: Present and future
1266 storm impact, *Ocean Dynamics* 60, 227 – 236.
1267

1268 Brown, J.M., Wolf, J., Souza, A.J., 2012. Past to future extreme events in Liverpool Bay: model projections
1269 from 1960 – 2000, *Climatic Change* 111, 365 – 391.
1270

1271 Callaghan, D.P., Nielsen, P., Short, A., and Ranasinghe, R., 2008. Statistical simulation of wave climate
1272 and extreme beach erosion, *Coastal Engineering* 55, 375 – 390.
1273

1274 Carter, R., 1988. *Coastal environments: an introduction to the physical, ecological and cultural systems of*
1275 *coastlines*, Academic Press, London, UK.
1276

1277 Ciavola, P., Jimenez, J.A., 2011. The record of marine storminess along European coastlines, *NHESS –*
1278 *Special Issue*, http://www.nat-hazards-earth-syst-sci.net/special_issue135.html
1279

1280 Dissanayake, D.M.P.K., 2011. *Modelling Morphological Response of Large Tidal Inlet Systems to*
1281 *Sea Level Rise*, PhD Dissertation, UNESCO-IHE Institute for Water Education, Delft, the Netherlands.
1282

1283 Dissanayake, D.M.P.K., Ranasinghe, R., Roelvink, J.A., 2012. The morphological response of large tidal
1284 inlet/basin systems to Relative Sea Level Rise. *Climatic Change*, DOI: 10.1007/s10584-012-0402-z
1285

1286 Dissanayake, D.M.P.K., Van der Wegen, M., Roelvink, J.A., 2009. Modelled channel pattern in a
1287 schematised tidal inlet, *Coastal Engineering* 56, 1069 – 1083.
1288

1289 Dissanayake, P., Wurpts, A., 2013. Modelling an anthropogenic effect of a tidal basin evolution applying
1290 tidal and wave boundary forcings: Ley Bay, East Frisian Wadden Sea, *Coastal Engineering* 82, 9 – 24.
1291

1292 Dolan, R., Davies, R.E., 1994. Coastal storm hazards, *Journal of Coastal Research* (Special Issue No. 12),
1293 103–114.
1294

1295 Donnelly, C., Kraus, N., Larson, M., 2006. State of knowledge on measurement and modelling of coastal
1296 overwash. *Journal of Coastal Research* 965 – 991.
1297

1298 Dronkers, J., 2005. Dynamics of Coastal Systems, *Advanced Series on Ocean Engineering – Volume 25*,
1299 235 – 240.
1300

1301 Edelman, T., 1968. Dune erosion during storm conditions, *Proceeding of the 11th conference of Coastal*
1302 *Engineering, London, Volume 2*, 719 – 722.
1303

1304 Edmondson, S.E., 2010. Dune Slacks on the Sefton Coast, Sefton’s Dynamic Coast, *Proceeding of the*
1305 *conference on coastal and geomorphology, biogeography and management*, 178 – 187.
1306

1307 Erikson, L., Larson, M., Hanson, H., 2007. Laboratory investigation of beach scarp and dune recession due
1308 to notching and subsequent failure. *Marine Geology* 245 (1), 1 – 19.
1309

1310 Esteves, L.S., Williams, J.J., Nock, A., Lymbery, G., 2009. Quantifying shoreline changes along the Sefton
1311 Coast (UK) and the Implications for Research-Informed Coastal Management, *Journal of Coastal*
1312 *Research, SI 56*, 602 – 606.
1313

1314 Esteves, L.S., Brown, J.M., Williams, J.J., Lymbery, G., 2012. Quantifying thresholds for significant dune
1315 erosion along the Sefton Coast, Northwest, England, *Geomorphology* 143 – 144, 52 – 61.
1316

1317 Esteves, L.S., Williams, J.J., Brown.J.M., 2011. Looking for evidence of climate change impacts in the
1318 eastern Irish Sea, *Natural Hazards Earth System Sciences*, 11, 1641 – 1656.
1319

1320 Galapatti, R., 1983. A depth integrated model for suspended transport. Report 83-7, Communications on
1321 Hydraulics, Department of Civil Engineering, Delft University of Technology.
1322

1323 Gold, I., 2010. LIDAR Quality Control Report Project PM_0901: Survey for Polygon P_6802,
1324 Environmental Agency, UK.
1325

1326 Gresswell, R.K., 1953. *Sandy Shores in South Lancashire*, Liverpool University Press, Liverpool.
1327

1328 Halcrow, 2009. North West England and North Wales Shoreline Management Plan 2, Appendix C:
1329 Baseline Processes, 40 pp (http://mycoastline.org/documents/AppendixC-C.4F_Seftoncoast.pdf).
1330

1331 Hallermeier, R.J., 1983. Sand Transport Limits in Coastal Structure Design, Proceedings, Coastal
1332 Structures '83, American Society of Civil Engineers, pp 703 – 716.
1333

1334 Harley, M.D. and Ciavola, P., 2013. Managing local coastal inundation risk using real-time forecasts and
1335 artificial dune placements, *Coastal Engineering* 77, 77 – 90.
1336

1337 Harley, M.D., Armaroli, C., Ciavola, P., 2011. Evaluation of XBeach predictions for a real-time warning
1338 system in Emilia-Romagna, Northern Italy. *Journal of Coastal Research*, Special Issue 64, 1861 – 1865.
1339

1340 Horsburgh, K.J., Wilson, C., 2007. Tide-surge interaction and its role in the distribution of surge residuals
1341 in the North Sea, *Journal of Geophysical Research*, Vol. 112, C08003, doi: 10.1029/2006JC004033.

1342

1343 Houston, J., 2010. The development of Integrated Coastal Zone Management (ICZM) in the UK: the
1344 experience of the Sefton Coast, Sefton's Dynamic Coast, Proceeding of the conference on coastal and
1345 geomorphology, biogeography and management, 289 – 305.

1346

1347 Jones, J.E., Davies, A.M., 1998. Storm surge computations for the Irish Sea using a three-dimensional
1348 numerical modelling including wave-current interaction, *Continental Shelf Research* 18, 201 – 251.

1349

1350 Karunaratna, H., Pender, D., Ranasinghe, R., Short, A.D., Reeve, D.E., 2014. The effects of storm
1351 clustering on beach profile variability, *Marine Geology* 348, 103 – 112.

1352

1353 Larson, M., Kraus, N., 1989. SBEACH: numerical model for simulating storm-induced beach change.
1354 Report 1: Empirical Foundation and Model Development, Technical Report, CERC-89-9. US Army
1355 Engineer Waterways Experiment Station, Vicksburg, MS. 267 pp.

1356

1357 Larson, M., Wise, R.A., Kraus, N., 2004. Modelling dune response by overwash transport. In: Mckee Smith,
1358 J. (Ed), *Coastal Engineering 29th International Conference*, World Scientific, Lisbon, Portugal, pp. 2133
1359 – 2145.

1360

1361 Lesser, G., Roelvink, J.A., Van Kester, J.A.T.M., Stelling, G.S., 2004. Development and validation of a
1362 three dimensional morphological model, *Coastal Engineering* 51, 883 – 915.

1363

1364 Lindemer, C., Plant, N., Puleo, J., Thompson, D., Wamsley, T., 2010. Numerical simulation of a low-lying
1365 barrier island's morphological response to Hurricane Katrina, *Coastal Engineering* 57 (11), 985 – 995.

1366

1367 McAleavy, D., 2010. Sefton Beach Management – Twenty Years of Progress, Sefton's Dynamic Coast,
1368 Proceeding of the conference on coastal and geomorphology, biogeography and management, 318 –
1369 326.

1370

1371 McCall, R., Van Thiel de Vries, J., Plant, N., Van Dongeren, A., Roelvink, J., Thompson, D., Reniers, A.,
1372 2010. Two-dimensional time dependent hurricane overwash and erosion modelling at Santa Rosa
1373 Island, *Coastal Engineering* 57 (7), 668 – 683.

1374

1375 Palmer, M.R., 2010. The modification of current ellipses by stratification in the Liverpool Bay ROFI,
1376 *Ocean Dynamics* 60, 219 – 226. doi 10.1007/s10236-009-0246-x

1377

1378 Palmsten, M., Holman, R., 2012. Laboratory investigation of dune erosion using stereo video, *Coastal*
1379 *Engineering* 60, 123 – 135.

1380

1381 Parker, W.R., 1969. A Report on Research Conducted into Aspects of the Marine Environment Affecting
1382 Coast Erosion between Ainsdale and Hightown, Lancashire, Lancashire County Council, pp 99.

1383

1384 Pender, D., Karunarathna, H., 2013. A statistical-process based approach for modelling beach profile
1385 variability, *Coastal Engineering* 81, 19 – 29.

1386

1387 Plater, A.J., Grenville, J., 2010. Liverpool Bay: linking the eastern Irish Sea to the Sefton Coast, Sefton's
1388 Dynamic Coast, Proceeding of the conference on coastal and geomorphology, biogeography and
1389 management, 41 – 43.

1390 Pye, K., Blott, S.J., 2010. Geomorphology of Sefton Coast and dunes, Sefton's Dynamic Coast, Proceeding
1391 of the conference on coastal and geomorphology, biogeography and management, 131 – 159.

1392

1393 Pye, K., Blott, S.J., 2008. Decadal-scale variation in dune erosion and accretion rates: an investigation of
1394 the significance of changing storm tide frequency and magnitude on the Sefton Coast, UK.
1395 *Geomorphology* 102, 652 – 666.

1396

1397 Pye, K., Neal, A., 1994. Coastal dune erosion at Formby Point, north Merseyside, England: causes and
1398 mechanisms. *Marine Geology* 119, 39 – 56.
1399

1400 Pye, K., Smith, A.J., 1988. Beach and dune erosion on the Sefton Coast, Northwest England, *Journal of*
1401 *Coastal Research*, SI. 3, 33 – 36.
1402

1403 Pugh, D.T., 1987. *Tides, Surges and mean sea level rise: a hand book for engineers and scientists* (472).
1404 Chichester: Wiley.
1405

1406 Ranasinghe, R., Callaghan, D., Stive, M.J.F., 2011. Estimating coastal recession due to sea level rise:
1407 beyond the Bruun rule, *Climatic Change*, DOI 10.1007/s10584-011-0107-8.
1408

1409 Roelvink, J.A., 2006. Coastal morphodynamic evolution techniques, *Coastal Engineering* 53, 277 – 287.
1410

1411 Roelvink, D., Reniers, A., van Dongeren, A., Van Thiel de Vries, J., McCall, R., Lescinski, J., 2009.
1412 Modelling storm impacts on beaches, dunes and barrier islands. *Coastal Engineering* 56, 1133 – 1152.
1413

1414 Roelvink, J., Stive, M.J.F., 1989. Bar-generating cross-shore flow mechanisms on a beach. *Journal of*
1415 *Geophysical Research* 94 (C4), 4785 – 4800.
1416

1417 Smith, P.H., 2010. Dragonflies (Odonata), *Proceeding of the conference on coastal and geomorphology,*
1418 *biogeography and management*, 175 – 177.
1419

1420 Soulsby, R., 1997. *Dynamics of marine sands*. Thomas Telford Publications, London, ISBN 0 7277 2584
1421 X.
1422

1423 Sallenger, A., 2000. Storm impact scale for barrier islands. *Journal of Coastal Research* 16 (3), 890 – 895.
1424

1425 Souza, A.J., Brown, J.M., Williams, J.J., Lymbery, G., 2013. Application of an operational storm coastal
1426 impact forecasting system, *Journal of Operational Oceanography*, Vol. 6, 23 – 26.
1427

1428 Splinter, K.D., Palmsten, M.L., 2012. Modelling dune response to an East Coast Low. *Marine Geology* 329
1429 – 331, 46 – 57.
1430

1431 Stive, M.J.F., Wind, H.G., 1986. Cross-shore mean flow in the surfzone. *Coastal Engineering* 10, 325 –
1432 340.
1433

1434 Thomas, C.G., Spearman, J.R., Turnball, M.J., 2001. Historical morphological change in the Mersey
1435 Estuary. *Continental Shelf Research*, 22: 1775-1794.
1436

1437 Van Rijn, L. C., Walstra, D.J.R., Grasmeyer, B., Sutherland, J., Pan, S., Sierra, J.P., 2003. The
1438 predictability of cross-shore evolution of sandy beaches at the scale of storm and seasons using process-
1439 based profile models. *Coastal Engineering* 47, 295-327.
1440

1441 Van Thiel de Vries, J.S.M., Van Gent, M.R.A., Walstra, D.J.R., Reniers, A.J.H.M., 2008. Analysis of dune
1442 erosion processes in large-scale flume experiments, *Coastal Engineering* 55 (12), 1028 – 1040.
1443

1444 Vellinga, P., 1986. Beach and dune erosion during storm surges. Delft University of Technology, PhD
1445 Thesis.
1446

1447 White, S., 2010. The Birds of the Sefton Coast: A review, Proceeding of the conference on coastal and
1448 geomorphology, biogeography and management, 162 – 173.
1449

1450 Williams, J.J., Brown, J., Esteves, L.S., Souza, A., 2011. MICORE WP4 Modelling coastal erosion and
1451 flooding along the Sefton Coast NW UK, Final Report (<http://www.micore.eu>).
1452

1453 Wolf, J., 1981. Surge-tide interaction in the North Sea and River Thames, in *Floods due to High Winds and*
1454 *Tides*, edited by D.H. Peregrine, pp. 75 – 94, Elsevier, New York.

1455

1456 Wolf, J., Brown, J.M., Howarth, M.J., 2011. The wave climate of Liverpool Bay – observations and
1457 modelling, *Ocean Dynamics* 61, 639 – 655.

1458

1459 Wolf, J., Woolf, D.K., 2006. Waves and climate change in the north-east Atlantic. *Geophysical Research*
1460 *Letter* 33:L06604, doi: 1029/2005GL025113.

1461

1462 Woodworth, P.L., Flather, R.A., Williams, J.A., Wakelin, S.L., Jevrejeva, S., 2007. The dependence of UK
1463 extreme sea levels and storm surges on the North Atlantic Oscillation, *Continental Shelf Research* 27
1464 (7), 935 – 946.